Energy & Environmental Science

ROYAL SOCIETY OF CHEMISTRY

PAPER

View Article Online
View Journal | View Issue

Cite this: *Energy Environ. Sci.*, 2025, **18**, 6043

Techno-economic and life-cycle assessment for syngas production using sustainable plasma-assisted methane reforming technologies

Marc Escribà-Gelonch, †[a] Jose Osorio-Tejada, †[bc] Le Yu, [d] Bart Wanten, [e] Annemie Bogaerts *[e] and Volker Hessel *[d]

This study combines for the first time techno-economic and life-cycle assessment metrics to evaluate the economic and environmental viability of plasma-assisted dry reforming of methane (DRM) for producing syngas from methane-rich natural gas. The study compares three different processes (plasma-assisted dry reforming (CO_2/CH_4), oxi-CO_2 reforming ($CO_2/CH_4/O_2$) and bi-reforming ($CO_2/CH_4/H_2O$)), as well as current state-of-the-art steam reforming technology. Advancements in cost reduction and environmental performance are highlighted. While comparative studies on different plasma processing concepts have been published, their number is not large; meaning this study is bespoke in this aspect. Our study is also bespoke in terms of the extensive consideration of industrial gas separation, providing a holistic view on sustainability with an industrial viewpoint. Three different production design scenarios were considered in the analysis: DRM (scenario 1), oxy-CO_2 reforming of CH_4 (OCRM) (scenario 2), and bi-reforming of CH_4 (BRM) (scenario 3). This evaluation was carried out through techno-economic analysis and a cradle-to-gate life cycle assessment (LCA). Among the scenarios analysed, OCRM demonstrates the most favourable economic performance, leading to a unitary cost of production of $549 per tonne syngas, followed by DRM and BRM. However, when operating at large scale, the syngas production cost of BRM could compete with the benchmark if 20% reduction in plasma power consumption can be achieved, so in the near future, plasma-based BRM could be competitive against other more mature electric-powered technologies. When assessing environmental performance across 10 environmental categories of LCA metrics, OCRM is again preferred, followed by DRM and BRM. Key impact categories identified include freshwater eutrophication potential and energy consumption, which are significant contributors to environmental impacts. A study on the transition of energy sources indicates a substantial decrease in global environmental impact in the range of 50% when shifting from current electricity generation methods to wind energy sources. Comparative benchmarking reveals that the technologies evaluated in all three plasma scenarios perform better in environmental metrics across 7 over 9 categories assessed, when compared with current state-of-the-art steam reforming technologies. A material circularity indicator around 0.7 is obtained in all scenarios with slight differences, reflecting a medium-high level of circularity. Sectors such as chemicals and recycling manufacturing could greatly benefit from our findings on plasma-assisted methane reforming. By leveraging these technologies, the energy industry can facilitate a shift toward renewable energy sources, enabling cost-effective and environmentally friendly production.

Received 2nd November 2024,
Accepted 17th April 2025

DOI: 10.1039/d4ee05129g

rsc.li/ees

Broader context

Transforming methane-rich natural gas into usable fuels and chemicals in a cleaner, more sustainable way is a growing priority for society. Plasma-assisted dry reforming of methane (DRM) is one such method that uses methane from natural gas to produce syngas, a key ingredient in many industrial processes. Unlike

[a] *Department of Environment, Soil Sciences and Chemistry, University of Lleida, Lleida, Spain*
[b] *School of Engineering, University of Warwick, Warwick, UK*
[c] *Faculty of Environmental Sciences, Universidad Tecnológica de Pereira, Pereira, Colombia*
[d] *School of Chemical Engineering, University of Adelaide, Adelaide, Australia. E-mail: volker.hessel@adelaide.edu.au*
[e] *Department of Chemistry, Research Group PLASMANT, University of Antwerp, Antwerp, Belgium. E-mail: annemie.bogaerts@uantwerpen.be*
† First authors

traditional steam reforming, which consumes a lot of water and energy, plasma-based DRM has the potential to be a greener alternative. This study compares plasma-based DRM with other innovative plasma approaches, like oxy-CO_2 reforming (OCRM) and bi-reforming (BRM), to evaluate which one is best for the environment and the economy. We studied the entire process, from production to the environmental impact, focusing on how renewable energy could make these methods even better. Our findings note that OCRM currently stands out as the most cost-effective and environmentally friendly option, but under large-scale conditions, BRM could become just as affordable, especially if powered by electricity from renewable sources. On the environmental side, OCRM has the smallest overall impact, followed by DRM and BRM. Key challenges, such as water pollution and high energy use, are identified, but switching to wind power could cut these impacts in half, highlighting the importance of clean energy. This research shows how to use resources responsibly, besides a simple pollution reduction, and how renewable energy and innovative processes like plasma-based DRM, OCRM and BRM can move closer to a cleaner, more circular economy.

1. Introduction

The increasing trend of greenhouse gas (GHG) emissions generated from fossil fuel utilization leads to a severe climate impact and significant carbon waste.[1] It is reported that the total global energy-based carbon dioxide (CO_2) emissions grew by 1.1% in 2023, reaching a record of 37.4 billion tonnes (Gt).[2] Methane (CH_4) and CO_2 are two major contributors to GHG emissions, posing potential risks for energy-related industries.[3] There is an imperative need for a mature and cost-effective process to convert CO_2 and CH_4 into useful products (*e.g.*, syngas and synthetic fuels) for downstream chemical industries. Among the useful products, syngas is considered the key intermediate product to generate other clean fuels, including methanol (CH_3OH) and dimethyl ether (DME).[4] It is also a primary chemical precursor for the refining process.[5,6] CH_4 reforming is the most-established approach for syngas production (Aramouni *et al.*, 2018[6]). Steam reforming of CH_4 (SRM, reaction (1)), dry reforming of CH_4 (DRM, reaction (2)), and oxy-CO_2 reforming of CH_4 (OCRM, reaction (3)) are three main methods for syngas production.[7] Other processes, such as bi-reforming of CH_4 (BRM, reaction (4)) and autothermal reforming (reaction (5)), are derived from these technologies.

$$CH_4(g) + H_2O(g) \rightleftharpoons CO(g) + 3H_2(g) \quad \Delta H^\circ = +206.1 \text{ kJ mol}^{-1} \tag{1}$$

$$CH_4(g) + CO_2(g) \rightleftharpoons 2CO(g) + 2H_2(g) \quad \Delta H^\circ = +247.3 \text{ kJ mol}^{-1} \tag{2}$$

$$3CH_4(g) + CO_2(g) + O_2(g) \rightleftharpoons 4CO(g) + 6H_2(g) \quad \Delta H^\circ = +175.9 \text{ kJ mol}^{-1} \tag{3}$$

$$3CH_4(g) + 2H_2O(g) + CO_2(g) \rightleftharpoons 4CO(g) + 8H_2(g) \quad \Delta H^\circ = +659.5 \text{ kJ mol}^{-1} \tag{4}$$

$$3CH_4(g) + H_2O(g) + O_2(g) \rightleftharpoons 3CO(g) + 7H_2(g) \quad \Delta H^\circ = +134.7 \text{ kJ mol}^{-1} \tag{5}$$

Among these reforming techniques, SRM converts CH_4 into carbon monoxide (CO) and hydrogen (H_2) using steam, producing a H_2/CO ratio of 3, which is unsuitable for the Fischer–Tropsch (F–T) process.[8] Its increased heat load for the endothermic reaction also requires a relatively high energy consumption. Recently, DRM has gained great attention as an attractive alternative for SRM, because it converts CH_4 and CO_2 (at equal conversion) into the production of H_2/CO with a ratio close to 1.[3,9] Moreover, DRM is more practical than other reforming processes, as there is no separation process needed for the outflow, which favours biogas (mixture of CO, CO_2 and CH_4) production for the development of renewable energy.[10] To some extent, this could bring the opportunity for carbon footprint mitigation of syngas production. Its tunable H_2/CO ratio by producing H_2 and CO_2 in the water-gas shift (WGS) reaction provides benefits for CH_3OH synthesis.[11] However, it is a reversible endothermic reaction that is thermodynamically activated between 640–900 °C, due to the harsh requirement (high energy) for CO_2 activation.[12] The main challenge that prevents the use of classical (thermocatalytic) DRM is coke formation and sintering, resulting in rapid deactivation of the catalysts.[13]

The OCRM process has been introduced to promote the energy efficiency by the addition of oxidants like oxygen (O_2) into the DRM feed, as the exothermicity created from partial oxidation of CH_4 provides the adequate heat demand for the DRM reaction.[12,14] The presence of O_2 can significantly suppress coke formation and modulate the heat from DRM to stabilize the particle size and morphology of the active catalyst phase.[15] Moreover, the use of OCRM can increase the process flexibility by tailoring the H_2/CO ratio that enables syngas into liquid hydrocarbon synthesis.[16] Compared to SRM and DRM, OCRM is more promising for syngas production, as the H_2/CO ratio of 1.5 that can be obtained by this method is suitable for the production of a variety of value-added chemicals. However, this process needs an extremely high reaction temperature up to 1200 °C to maintain a high conversion of CH_4.[17] Thermocatalytic OCRM is applied to lower the temperature with increased syngas selectivity at the same CH_4 conversion efficiency. Despite several studies focusing on favourable reaction kinetics, it is still challenging to widely commercialize this technology, as the H_2/CO ratio of 1.5 generated from OCRM still poses great limitations for industrial application.[18] Moreover, catalyst deactivation occurring during sintering can largely decrease the syngas selectivity with elevated reaction temperature, therefore causing important safety concerns.[7]

Recently, BRM has shown significant merits compared to DRM and OCRM, due to its ability of reducing carbon deposition and modifying the H_2/CO ratio, offering a more practical route for improving the H_2/CO ratio.[19] It is ideal for CH_3OH synthesis, since it can generate a high grade of syngas with a H_2/CO ratio of 2 using a mixture of CH_4, CO_2 and H_2O at a ratio of 3 : 1 : 2.[20] This high-grade syngas has potential towards the Fischer–Tropsch process for the preparation of long-chain

Table 1 Comparative techno-economic assessments of syngas production technologies proposed in this study

Parameter	Dry methane reforming (DMR)	Oxy-CO_2 reforming (OCRM)	Bi-reforming (BRM)
CO_2 utilization	High	Moderate	High
H_2/CO ratio	~1.1 (needs adjustment)	Adjustable	Ideal for syngas
Energy demand	High (especially plasma-assisted)	Moderate	High (due to steam requirement)
Capital cost	Moderate to high	High (oxygen separation)	Moderate
Economic viability	Competitive if electricity is cheap	Needs cost-effective O_2	Competitive with SMR

hydrocarbon products.[21] One study has claimed that a high conversion (90%) of CH_4 at a low reaction temperature (~480 °C) can be achieved by BRM coupling with a bubbling catalyst bed, providing a crucial alternative towards the conventional reforming process.[22] It is also reported that BRM can be used for biogas enhancement *via* the solar reforming process.[23] However, to develop this technology at the commercial level, a suitable catalyst for the BRM process needs to be investigated for promoting the reaction.

Regarding techno-economic assessments (TEA), a literature study demonstrates that while plasma-based DRM offers sustainability advantages,[24] it requires significantly more electricity (approximately 10 times more than of thermal catalytic DRM), making it less competitive unless electricity costs decrease substantially.[24] However, plasma-based DRM can simplify downstream processing by reducing production steps.[24] In this process, major contributors to the capital expenditure (Capex) include refrigeration systems, compressors, and plasma reactors, see Table 1. While thermal catalytic DRM relies on catalysts, plasma-assisted DRM reduces catalyst demand or even operates completely without catalysts, potentially lowering operating costs.[24] Plasma-based OCRM has been studied less extensively than DRM. The need for oxygen separation increases capital costs, making it more expensive than DRM.[25] Therefore, while the OCRM process itself can enhance efficiency, its economic competitiveness largely depends on oxygen production costs and overall energy consumption.[25] Plasma-based BRM includes features of steam methane reforming (SRM) and DRM, utilizing both H_2O and CO_2 to reform CH_4 into syngas. Studies indicate that for syngas production, its economic feasibility is comparable to conventional SRM.[26] When applying these findings to plasma-produced syngas, the high energy requirements underscore a strong dependence on electricity costs, which significantly influence economic feasibility. Additionally, the initial Capex remains a major barrier.[27] In terms of catalysis, while plasma-assisted syngas production could be enhanced through plasma catalysis, integrating catalysts into plasma processes is far more challenging than in conventional catalysis. Moreover, the expected synergy between plasma and catalysis is not always achieved, as the underlying mechanisms are still not well understood.

In terms of separation, while plasma-based syngas production simplifies downstream processing due to simplification driven by catalyst avoidance,[28] there are trade-offs in terms of operational efficiency, high electricity consumption and capital costs. Table 1 compares CO_2 utilization, the resulting H_2/CO ratio, energy demand, capital costs, and overall economic viability of the three plasma-based reforming processes evaluated in this study: DRM, OCRM, and BRM.[29]

Besides the proposed five reactions for syngas production, DRM, OCRM, and BRM are considered common alternatives for syngas production given the simultaneous conversion of both CO_2 and CH_4 in an oxidative environment with an ideal H_2/CO ratio in a single step.[30] Additionally, extensive studies by different technologies have been performed to assist the CH_4 reforming technology, including thermal catalysis, plasma technology and thermal pyrolysis, finding high potential to produce syngas in a practical way.[31] However, several problems have been revealed using thermal catalysis, such as carbon deposition, catalyst poisoning and sintering occurring at high temperature, leading to unsuitable commercial applications.[22] Thermal pyrolysis is also energy-intensive and synthesizes fewer value-added products compared to plasma technology.[32]

On the other hand, plasma-assisted CH_4 reforming has attracted great attention, due to numerous advantages of prompt response time, mild reaction circumstances, and compact size of the reactors.[33] Hence, plasma technology is currently considered a promising alternative for classical CH_4 reforming. Plasma technology involves a partially ionized gas, created by applying a potential difference between two electrodes, in between which a gas flows. It is divided into three categories, *i.e.*, thermal, non-thermal and warm plasma. In non-thermal and warm plasmas, the gas is in non-equilibrium with the electron temperature. The gas temperature can vary from room temperature up to above 1000 K.[34,35] There are some key advantages that make non-thermal or warm plasma attractive for CH_4 reforming, including: (1) it provides a high energy density for endothermic reactions; (2) it provides a high amount of chemically energy-active species to accelerate the reaction; (3) the non-equilibrium between electron and gas temperature avoids thermodynamic equilibrium, which maintains the reaction at mild conditions, (4) it does not require catalysts or expensive materials for the reactors, (5) it is very flexible in terms of feed and products, (6) it is a continuous process (flow reactors), (7) it can be upscaled by numbering-up, but can also operate at small scale (no economy of scale), and last but not least (8), it is created by applying electricity and can quickly be switched on/off, so it is very suitable for combination with renewable electricity, hence for electrifying chemical reactions (Chung and Chang, 2016;[35] Bogerts and Neyts, 2018[36]).

Several plasma reactors for CH_4 reforming have been extensively investigated during the last decade.[37,38] Despite its promising outcomes, plasma-assisted CH_4 reforming is complex, as the discharge parameters can impact the conversion and product distribution upon ionization and excitation of

the gas species.[39] For instance, some gliding arc plasma reactors suffer from low conversion, as a fraction of the feed gas cannot pass the active plasma zone.[40,41] Dielectric barrier discharges are often used due to their simple configuration, enabling catalyst particles to be introduced into the reactor volume,[42] and because they can easily control the plasma system with high scalability.[43] However, their energy cost for CH_4 reforming is too high to be competitive with other technologies.[37,44] Recently, the performance of DRM in an atmospheric pressure glow discharge (APGD) was investigated,[38] and the total conversion could reach 74% with an energy cost below 4.27 eV per molecule, which is defined as the target for plasma-based DRM to be competitive with other emerging technologies.[37,38] This confined APGD plasma reactor was later also applied to other CH_4 reforming processes, such as BRM and OCRM, to achieve the targeted H_2/CO ratio with lower carbon deposition and avoiding plasma instability.[45,46]

Sustainability studies, with rare exceptions, have to face the challenges of data reliability and accountability, especially when dealing with emerging technologies and highly innovative translation into industrial settings. Often, for example, only laboratory data are available. Yet, the success of flow chemistry used by the pharmaceutical industry was notably propelled by sustainability assessments with the same limitations.[47] The way out of this intrinsic dilemma can be manifold. Our concept, published multiple times,[28,48,49] is to use laboratory data, add our own pilot data wherever accessible,[50] and to scale these data using lead expertise in scaling up emerging technologies.[51] This generally works well with mass flow data, and, honestly, scaled-out energy/power data are not as reliable. In the next paragraph, we illuminate the expertise in scaling up, in terms of the pros and cons.

Scaling up plasma reactors is challenging due to issues in maintaining mass and heat transfer.[28,48] Common strategies include increasing reactor volume by enlarging tubing or connecting reactors in series, but plasma reactor performance depends on geometry. An alternative is numbering-up, where multiple reactors operate in parallel.[51,52] This can be external (separate reactor shells) or internal (multiple zones in one shell). Scaling also requires considerations for gas handling, power supply, and safety. Industrial-scale reactors face added complexities like energy distribution and gas flow variability. Despite these challenges, upscaled plasma technologies are used in microelectronics, ozone generation, and combustion.[53,54] Industrial reactors must handle feedstock variability and must ensure long-term operational stability, which is clearly different from lab-scale systems.

Policies such as the European Green Deal and the goal of reducing emissions by 55% aim to accelerate decarbonization. While the Green Deal itself does not explicitly propose plasma-assisted reforming, innovative technologies like plasma technology can contribute to improving energy efficiency and resource utilization in line with broader sustainability goals. Additionally, the Green Deal promotes investment in research and development for cutting-edge climate solutions, creating opportunities for emerging technologies to support the transition to a low-carbon economy. By aligning with these priorities, advancements in this field can achieve sustainability targets in the future. The environmental impacts associated with these technologies are of course equally crucial as technological advancements in achieving sustainability, particularly in meeting the sustainable development goal (SDG) number 12, related to responsible consumption and production, since both CO_2 and CH_4 are highly relevant when considering the global warming potential (GWP) environmental category. Recent life cycle assessment (LCA) studies have focused on evaluating the carbon footprint of novel technologies compared to traditional methods for syngas production.[55,56] As an example, Choe *et al.*, (2022)[57] examined the potential of emerging solid oxide electrolysis to generate syngas using various renewable energy sources, including hydropower, onshore and offshore wind, solar photovoltaic (PV), bioenergy, and geothermal energy, concluding that syngas production from onshore wind, offshore wind, solar PV, and geothermal energy offers environmental benefits over syngas produced from fossil fuels. Likewise, Sternberg and Bardow, (2016)[58] conducted a comparative study of syngas production methods, comparing DRM and reverse water-gas-shift (rWGS) with conventional SRM, concluding that rWGS (5.8 kg CO_2 eq. per kg syngas, 1.9 kg oil eq. per kg syngas) and DRM (4.2 kg CO_2 eq. per kg syngas, 1.5 kg oil eq. per kg syngas) have higher global warming and fossil resource scarcity impacts than conventional SRR (2.5 kg CO_2 eq. per kg syngas, 1.2 kg oil eq. per kg syngas), primarily due to the high electricity consumption of the proton exchange membrane (PEM) electrolysis unit. In other cases, biochemical approaches have been considered, such as comparing biogas with natural gas reforming,[59] assessing the water footprint of biomass chemical looping gasification,[60] and comparing thermo- and bio-chemical routes for biowaste gasification.[61]

Due to the high energy demands of conventional gasification and DRM processes, which operate at high temperatures (800–1000 °C), many innovative approaches have been developed, trying to reduce the environmental impact of these demands. Despite the high efficiency of processes such as photocatalytic DRM for syngas production, the life cycle sustainability still remains uncertain, limiting its practical application.[58,59,62,63] Environmental considerations are often overlooked when transitioning from the experimental stage to practical application.

Dry reforming of methane (DRM), *i.e.*, the combined conversion of CO_2 and CH_4, has several advantages compared to pure CO_2 splitting and CH_4 pyrolysis. First, the reaction enthalpy is lower than for CO_2 splitting, and thus, the reaction can proceed at lower temperature. Second, the main product, syngas (mixture of CO and H_2) is an important precursor for the production of several highly valuable chemicals. Third, and most importantly, DRM allows the use of a biogas mixture, which mainly consists of CO_2 and CH_4, and removes the need to separate CO_2. However, classical (thermo-catalytic) DRM is not widely used on an industrial level, mainly because of extensive soot formation, which often leads to catalyst poisoning. For this reason, research on applying alternative methods for DRM is conducted, including plasma technology, where

soot formation can be reduced, among others also by mixing with O_2 or H_2O vapor, as in oxi-CO_2 reforming of methane (OCRM) and bi-reforming of methane (BRM), as demonstrated in this paper.

It should however be noted that plasma operations generally are at an infancy or best pilot stage, making it difficult to judge societal and industrial relevance. The best approximation is to judge the latter based on the available data of conventional (steam) reforming of methane (SRM), in the hope that the same societal and industrial benefits can be garnered. For SRM and its economic relevance, the global syngas market demand is expected to grow at a CAGR of 11.3% from 2024 to 2030, reaching 230.05 million $Nm^3\ h^{-1}$ already in 2023.[64] Concerning societal relevance, syngas is essential for ammonia synthesis *via* the Haber–Bosch process, which underpins global agricultural productivity.[65] Without ammonia-based fertilizers, modern agriculture could not sustain the current global population. Syngas is also a precursor for methanol, a versatile chemical used in the everyday life of the globe's customers, *e.g.*, as an antifreeze agent as well as key feedstock for producing formaldehyde, acetic acid, and a variety of plastics and synthetic materials.[66]

Only a few studies have addressed the environmental impact and carbon emission of plasma-assisted SRM *via* LCA,[67,68] and no studies have been reported on plasma-assisted DRM.[69] In order to address this gap in existing research, this paper evaluates the sustainability performance of plasma-assisted DRM, BRM, and OCRM by integrating techno-economic analysis and sustainability assessments, using a combination of laboratory-scale experiments and simulation data, to evaluate the economic and environmental feasibility of three different plasma-assisted methane reforming technologies compared to conventional methods, highlighting advancements in cost reduction and environmental performance.

2. Material and methods

2.1. Process description

2.1.1. Process feeds and products. The compositions of the feed varied based on the three different processes investigated, including DRM (scenario 1), OCRM (scenario 2) and BRM (scenario 3). Scenario 1: the feed gas to the process was set as 28% CH_4 and 72% CO_2 by mass, based on the APGD plasma-based experiments,[38] followed by WGS reaction, and the resulting gas was obtained after dual pressure swing adsorption (PSA) to reach a H_2/CO molar ratio of 1. Scenario 2: with the same process and condition, the feed gas to the process was set as 36% CH_4, 48% CO_2 and 16% O_2 by mass, and the resulting gas product was kept the same, *i.e.*, with a H_2/CO molar ratio of 1.[46] Scenario 3: the feed gas to the process was set as 44% CH_4, 27% CO_2 and 29% H_2O by mass, used for the APGD plasma-based reaction without WGS, and the resulting gas was obtained after the PSA process at a H_2/CO molar ratio of 2.[45]

2.1.2. Process design. The process design for scenario 1 and 2 was composed of the APGD plasma-based reaction, WGS reaction, gas cleanup and dual PSA system. The APGD plasma reactor consists of a cathode pin and anode plate, and details of this device can be found in a previous study.[38] Initially, a high voltage of 30 kV (40 mA) was supplied by a Technix DC power supply for plasma ignition, and then it dropped to 10–15 kV for stable plasma operation. The flow rate of the feed gas was regulated by mass flow controllers. Nitrogen (N_2) was added to the resulting gas mixture to account for gas expansion, which is crucial for accurate measurement of gas conversion and product yields.[70] The WGS reaction was applied to improve the H_2/CO ratio to a useful ratio of 1, at a temperature of 400 °C and reaction efficiency of 90%. After the reaction, the gas mixture was subject to cooling (25 °C) to remove H_2O traces. To achieve high purity of the gas product, dual PSA as a promising membrane purification method was used to separate O_2 and recover H_2. Scenario 3 used the same process but without the WGS system.

The process design for scenario 1 and 2 was composed of the APGD plasma-based reaction, WGS reaction, gas cleanup and dual PSA system. The APGD plasma reactor that was used for this study was originally investigated by Trenchev *et al.*, (2019),[71] where it was applied towards CO_2 splitting. Specifically, it consists of a cathode pin and anode plate, both made from stainless steel (Therma 310S). The cathode and plasma region are surrounded by a tube made of MACOR® machinable ceramic, with an inner radius of 2.5 mm, which is sufficiently heat resistant against the nearby plasma. The cathode contains a groove of ±1 mm depth, through which the gas enters the discharge zone. This provides a vortex flow and a high gas velocity close to the cathode, to effectively cool the latter, as well as the ceramic tube. The anode plate is positioned at the end of the ceramic tube, at 22 mm from the cathode tip, and contains an opening in the center through which the gas can exit the reactor. This "confined" design has led to a significant CO_2 conversion at a reasonably high energy efficiency (the definitions of the performance metrics are described by Wanten *et al.*, (2023).[70] Even better results were obtained by adding CH_4 and applying this reactor towards DRM (scenario 1), OCRM (scenario 2) and BRM (scenario 3). With these experiments, a high voltage of 30 kV (40 mA) was supplied by a Technix DC power supply for plasma ignition, and then it dropped to 10–15 kV for stable plasma operation. The flow rate of the feed gas was regulated by mass flow controllers. For the BRM experiments (scenario 3), CO_2 and CH_4 were mixed with heated de-ionized water before entering the reactor. Gas expansion was appropriately taken into account, *e.g.* by adding nitrogen (N_2) to the resulting gas mixture, which is crucial for accurate measurement of gas conversion and product yields.[70] More details of the lab-scale experiments with this reactor can be found in previous studies.[38]

Commonly, the power reported in the literature for plasma-based gas conversion is the plasma-deposited power. This neglects energy losses from the plug to the plasma, *i.e.* energy losses in the power supply and other electrical components.[70] For the lab-scale experiments with the atmospheric pressure glow discharge reactor, a Technix DC power supply (with a measured efficiency of 70–80%) was used to ignite and sustain

the plasma. Additionally, a ballast resistor of 300 kΩ (scenario 1 & 2) and 100 kΩ (scenario 3) was used in between the power supply and the reactor's cathode, thereby limiting and stabilizing the current. Despite its simplicity and practical use on lab scale, these ballast resistors dissipate a large fraction of the supplied energy as heat due to the Joule effect, leading to significant additional energy losses (Renninger *et al.*, 2020).[72] Therefore, when the LCA calculations are only based on the deposited plasma power, it would lead to an overestimation of the energy efficiency of the overall process, because the efficiency of the power delivery from the plug to the plasma should be considered as well.

In this regard, the lab scale setup was not optimized. Therefore, we need to have a realistic indication of how much the efficiency can be improved, in order to use a realistic plug power for each scenario. First of all, the ballast resistors can be avoided. The topology of switching mode power supplies can be optimized in order to significantly reduce the energy losses. Typically, a MOSFET (metal–oxide–semiconductor field-effect transistor) is used together with a diode, inductor and capacitor. The inductor stores the energy in a magnetic field during the charging phase instead of dissipating it as heat (which is done by a resistor), and thus the efficiency can be drastically improved while still allowing sufficient current control.[73]

For example, Renninger *et al.*, (2020)[72] used a power supply with a flyback driver and an inductor with no ballast resistors for an atmospheric pressure glow discharge for CO_2 conversion. They mentioned that for a scaled-up system, the efficiency (in terms of plasma-deposited power relative to supplied power) could be improved up to 80–90%. O'Modhrain *et al.* (2024)[50] used low-cost power supply units (PSU) again with a switching topology, allowing a current-regulated output without the need for a ballast resistor. Albeit applied for an arc discharge, the PSU's operate with an efficiency of *ca.* 80% and they stated that this can be improved further over 90%. It should be noted that both these power supplies are specifically designed for their corresponding setups. Therefore, when a power supply is specifically designed and optimized for this reactor we can assume similar efficiencies for this work (80%).

2.2. Techno-economic analysis

This analysis was performed to estimate the unitary cost of production (UCOP) per tonne of syngas in each of the three scenarios. The UCOP was estimated as the sum of the annual operating expenditure (Opex) and the annualised capital cost (ACC) divided by the annual syngas production.[74] The ACC was calculated based on the total fixed Capex, considering a 20-year lifespan (n) and 10% interest rate (i), as presented in eqn (6) and (7).

$$\mathrm{UCOP} = \frac{\mathrm{Opex} + \mathrm{ACC}}{\text{annual plant capacity}} \tag{6}$$

$$\mathrm{ACC} = \frac{[i(1+i)^n]}{[(1+i)^n - 1]} \times \mathrm{Capex} \tag{7}$$

Capex was calculated based on the uninstalled cost of the different equipment from literature specifying a reference capacity and year. Subsequently, the reference costs were scaled up/down to the required size and updated to US$$2020 prices based on the chemical engineering plant cost indices (CEPCI),[75] as presented in eqn (8). A currency exchange of €1.142 per $ was used when required.

$$C_B = C_A \left(\frac{S_B}{S_A}\right)^N \times \frac{\mathrm{CEPCI}_{2020}}{\mathrm{CEPCI}_{year}} \tag{8}$$

C_B represents the updated cost of the uninstalled equipment to the required capacity; S_B is the required capacity of the equipment; C_A is the reference cost of the equipment with specific capacity S_A, and N is the scaling exponent indicated for each equipment. For our plants, these scaling exponents were mostly between 0.6 and 0.9. This equipment cost estimation is based on 'the Rule of Six-tenths' approach.[76] The reference capacities, uninstalled costs, year, and scaling exponents are summarized in Table 2.

2.3. Life cycle assessment

Since LCA is a thorough and quantitative approach used to evaluate the environmental impacts associated with a process, product, or service,[47] conducted in accordance with

Table 2 Capacities, uninstalled costs, year, and scaling exponent of the process components

Equipment	Unit	Reference capacity	Reference uninstalled cost ($$)	Year	Scaling exponent	Ref.
APGD plasma setup	kW	5.6	7691	2020	**0.90**	O'Modhrain *et al.*, (2024)[50] and own data
Fired heater	kW	24 580	8 540 000	2018	**0.70**	Rezaei and Dzuryk, (2019)[77] and Hamelinck *et al.*, (2004)[78]
Heat exchanger	kW	59 540	3 000 000	2018	**0.62**	Rezaei and Dzuryk, (2019)[77] and Whitesides, (2012)[79]
Cooler	kW	5720	320 000	2018	**0.62**	Rezaei and Dzuryk, (2019)[77] and Whitesides, (2012)[79]
Low temp cooler	kW	1000	2 047 000[a]	2016	**0.63**	Luyben, (2017)[80]
Compressor	kW	12 490	5 460 000	2018	**0.67**	Rezaei and Dzuryk, (2019)[77] and Whitesides, (2012)[79]
Knockout drum	kg h^{-1}	99 795	157 277	2002	**0.60**	Spath *et al.*, (2005)[81]
Cyclone	m^3 s^{-1}	34.2	3 000 000	2016	**0.70**	Chiuta *et al.*, (2016)[82]
VPSA O_2 separation	m^3 h^{-1}	11 900	4 430 000	2020	**0.67**	Luberti and Ahn, (2021)[83]
WGS reactor	(H_2 + CO) kmol h^{-1}	8819	12 200 000	2002	**0.65**	Hamelinck *et al.*, (2004)[78] and Chiuta *et al.*, (2016)[82]
PSA syngas separation	m^3 h^{-1}	1000	1 998 500	2015	**0.67**	Paturska *et al.*, (2015)[84]

[a] Uninstalled cost was estimated by assuming a similar average ratio uninstalled/installed cost obtained for this study of 0.5.

ISO 14040-44 standards, it involves five essential steps:[85,86] (a) Defining the goal and scope, (b) defining the process boundaries, (c) conducting an inventory analysis, (d) performing an impact assessment, and (e) interpreting the results.

2.3.1. Goal and scope definition. The goal of this study is to investigate the environmental impact of three selected plasma-assisted CH_4 reforming technologies, compared to conventional SRM. This analysis was considered as a cradle-to-gate LCA study, using the data extracted from the laboratory scale. Downstream applications are excluded to avoid assumptions about specific uses of syngas (*e.g.*, methanol synthesis, Fischer–Tropsch synthesis), which vary in requirements (*e.g.*, H_2/CO ratios). This approach ensures comparability with conventional SRM and adheres to LCA best practices for assessing intermediate product impacts. Its system boundary included the feed input, energy flows into and out of the plasma reactor without transportation and plant construction, and the downstream processes, including gas cleanup, WGS system, cooling and drying, and dual PSA system. Transportation impacts were considered as equivalent in all cases, to focus on the process impacts, while construction impacts were considered as negligible when compared to the cumulative impacts over the lifetime of the infrastructure. Considering that the technology readiness level (TRL) of the APGD plasma process is still at the laboratory stage (TRL of 3), the energy efficiency and the gas conversion rate (per time) of these three processes were adapted from estimated data from the literature *in lieu* of the actual assessment. The obtained results of the above-mentioned processes were then benchmarked with the current SRM technology. The process information of SRM technology was obtained from the electrification of the endothermal reactor process described by Cao *et al.*, (2022),[87] involving all material input and energy consumption through the process for syngas production.

The functional unit is defined as 1 kg syngas production, and the energy required for the entire process is supplied *via* electricity from the European mixture standards (updated to 2023): renewable energy (43%), nuclear energy (28%), solid fuels (19%), natural gas (6%) and crude oil (3%).[88] The key environmental category of interest for this study is global warming potential (GWP) with the unit of kg CO_{2eq} per kg syngas produced. Carbon dioxide was taken as "liquid carbon dioxide production" also from Europe (RER) to prevent transport interactions. This source includes the material, energy inputs and emissions for CO_2 industrial production. "Biomethane sources" were considered for methane loadings at high pressure, to avoid transport interactions.

2.3.2. Process boundaries. The assessment within the cradle-to-gate boundary is carried out using the allocation at the point of the substitution (APOS) system model. This method aims to evaluate the life cycle impacts from the extraction of raw materials up to the processing of desired products, such as syngas, while also accounting for the generation of unwanted waste pollutants within the industrial gate. The analysis does not include potential aspects of the product distribution, consumption, or disposal. By focusing on the cradle-to-gate boundary, a thorough evaluation and comparison of both current and emerging syngas production systems is addressed. Fig. 1 illustrates the system boundaries and process flow for the three scenarios considered.

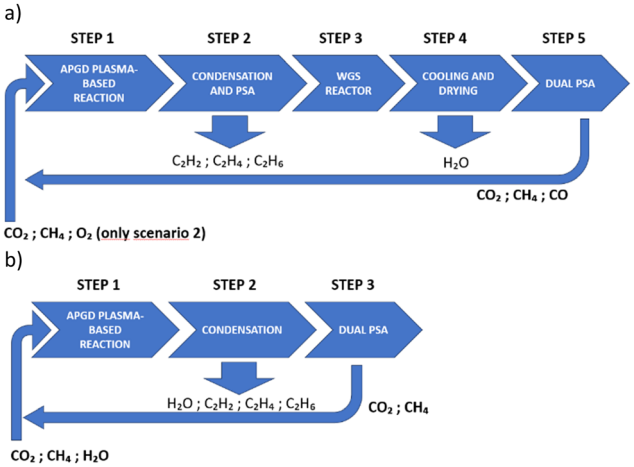

Fig. 1 Process scheme and scenarios definition. (a) Scenarios 1 and 2, and (b) scenario 3.

2.3.3. Life cycle inventory. The feed input, product composition, energy consumption, inventory data and process design conditions for three different scenarios, *i.e.*, DRM, OCRM and BRM, are listed in Tables 3 and 4.

2.3.4. Impact assessment. The detailed information of the inventory analysis is discussed in the Results and discussion section. We selected ten impact categories for the LCA analysis, including acidification potential (AP), climate change (global warming potential; GWP), freshwater ecotoxicity (FET), freshwater eutrophication (EPw), human toxicity including carcinogenic (HTc) and non-carcinogenic (HTnc), terrestrial eutrophication (EPt), non-renewable energy resources (fossil resources used; CEDf), material resources (metals/minerals) (CEDm) and photochemical ozone formation (Ph). The projected ecological impact of this research is afforded using EF3.1 environmental impact quantification, which refers to the standardized method developed under the European Commission's Environmental Footprint initiative.[89] Ecoinvent 3.10 is used for impacts comprehensive categorization. EF3.1 enhances the accuracy and comparability of environmental assessments by refining impact indicators and methodological guidelines, thereby enabling more effective identification and reduction of environmental burdens across supply chains.

2.3.5. Interpretation. During the LCA analysis, the data obtained from the literature were used with no further accuracy evaluation. All the raw data, such as feed gas and product gas, were obtained from the laboratory experiments.[38,45,46] However, to investigate the reliability of the LCA results, the uncertainty of analysis-related input flows was evaluated for all three plasma-assisted approaches. This analysis will be discussed and explained in the Results and discussion section. Importantly to note, our LCA studies show that OCRM is the most promising approach for syngas production, compared to DRM, although

Table 3 Feed input, product composition and energy consumption per kg syngas production of the various steps for the three plasma-based CH_4 reforming processes

Information		DRM	OCRM	BRM	SRM
Feed input (weight%)	CH_4	16.4	23.8	28.8	18.8
	CO_2	83.5	67.0	31.5	0.8
	O_2	—	9.1	—	—
	H_2O	—	—	39.6	74.5
	CO_2/CH_4 molar ratio	1.86	1.02	0.33	0.04
Syngas output (g)	CO	0.584	0.542	1.123	0.87
	H_2	0.042	0.039	0.157	0.13
	H_2/CO molar ratio	1.00	1.00	1.94	2.05
Energy consumption (kW h)	Plasma reaction	2.92×10^{-3}	1.96×10^{-3}	8.33×10^{-3}	
	Gas cleanup	6.05×10^{-4}	5.75×10^{-4}	6.23×10^{-4}	
	WGS reaction	2.48×10^{-4}	2.11×10^{-4}		
	Cooling & drying	2.76×10^{-5}	2.23×10^{-5}		
	Dual PSA system	4.55×10^{-4}	3.92×10^{-4}	9.88×10^{-4}	
	Total energy	$\mathbf{4.25 \times 10^{-3}}$	$\mathbf{3.16 \times 10^{-3}}$	$\mathbf{9.94 \times 10^{-3}}$	$\mathbf{10.4 \times 10^{-3}}$
Energy consumption	kW h per kg syngas	**6.69**	**5.35**	**7.75**	**6.5**

Table 4 Process design for the plasma-based CH_4 reforming process

Information	Unit	Plasma-based CH_4 reforming
APGD plasma reaction		
Temperature	°C	500
Electricity	W	400
Reaction efficiency	%	60
Gas cleanup		
Temperature	°C	−103
Condensation energy	kJ min^{-1}	1.9
Coefficient of performance	—	0.5
Cooling for gas flow	kJ min^{-1}	2.8
Water–gas shift		
Temperature	°C	400
Heating for gas mixture	kJ min^{-1}	0.7
Reaction efficiency	%	90
Total heating energy	kJ min^{-1}	0.8
Dual PSA system		
Temperature	°C	25
Reaction efficiency	%	90
Pressure	bar	23

the environmental impact assessment may not be fully comprehensive. Downstream processes were necessary for plasma-assisted CH_4 reforming technologies, including the WGS and dual PSA system, that are simultaneously performed after reforming of CH_4. The reaction efficiencies of all processes were adapted from the literature based on the reaction conditions. The BRM process was designed without the WGS system. Although it produced slightly higher climate impact compared to the other two processes, the molar ratio of the H_2/CO ratio equal to 2 was considered as an ideal approach to synthesize major gas-based chemicals, such as methanol and ethylene.

To guarantee the reliability of the outcomes of this assessment, it is crucial to acknowledge the intrinsic limitations and uncertainties relevant to the available literature sources. In particular, in terms of OCRM and BRM, further research and improvement for the processing data collection based on feed and energy flows can potentially contribute to enhanced accuracy and robustness of the comparison between SRM and plasma-assisted CH_4 reforming technologies.

2.4. Circularity of mass flow metrics

A circularity assessment utilizing circular economy metrics is designed to quantify the performance of products by assessing the extent of material and resource usage and reuse until they are fully exhausted. This process also evaluates the reduction of waste generation, aiming to promote a sustainable and regenerative economic system. By measuring aspects such as material efficiency, product lifespan extension, and waste minimization, these metrics support innovation by design, identifying opportunities for resource optimization and waste reduction throughout the product lifecycle. Integrating these metrics aids in the development of circular economy strategies focused on closed-loop systems, which reduce environmental impacts related to resource extraction and consumption, aligning with global sustainability objectives like the United Nations Sustainable Development Goals. The methodology proposed by the Ellen MacArthur Foundation (EMAF) is widely recognized for this purpose.[90] The calculation procedure includes several indices, converging on the material circularity indicator (MCI), which quantifies the restorative and regenerative nature of material flows on a scale from 0 (fully linear) to 1 (fully circular). The MCI is directly calculated as a function of LFI according to eqn (9) and (10). Further information about these equations is provided in Section 3.3.

$$MCI_P = 1 - (LFI \cdot F(X)) \tag{9}$$

$$\text{(a) } LFI = \frac{V + W}{2M + \frac{W_F}{2}}; \quad \text{(b) } F(X) = \frac{0.9}{\left(\frac{L}{L_0}\right) \cdot \left(\frac{U}{U_0}\right)} \tag{10}$$

This assessment approach has been applied in previous studies,[47,91] and recently to plasma-based CO production processes.[28]

Since there are no actual cost estimates for commercial-scale plants using the APGD plasma setup, the reference cost for this plasma section was based on a recent experience, where colleagues scaled up a gliding arc plasma prototype.[50] This prototype costs around €2400 per kW with a capacity of 5.6 kW of plasma power, capable of processing 6.7 tonnes of CO_2 per year, with future installation plans expected to process 30 000 tonnes of CO_2 per year.[28,50,92] The lower cost for the APGD plasma was estimated based on our current lab-scale setup, which had a cost of €17 900 for a maximum plasma power of 1.5 kW, compared to the lab-scale gliding arc setup, which had a cost of €24 800 for a maximum plasma power of 1 kW. It is also important to note that about 70% of the total cost of these plasma setups is due to the power supply unit (PSU). Therefore, the setup cost is primarily dictated by the required electric power, rather than the gas flow rate, as is typical for conventional reactors. This also explains the scaling exponent of 0.9 suggested by the manufacturer, which is appropriate for electronic devices, as opposed to the usual 0.6 exponent for reactors scaled up *via* volume expansion.

In this context, aside from using a different scaling exponent, the upscaling design of the plasma setup is also distinct, consisting of several reactor nodes in parallel instead of a single, large reactor scaled up using traditional methods. The most appropriate method in our case would be internal numbering up.[28,93] This method involves grouping several reactor nodes into a unified reactor body, powered by a single PSU, instead of using one PSU per reactor node (referred to as external numbering up). This method has already been tested by unifying five 1.1 kW reactor nodes in parallel, maintaining similar energy performance as the lab-scale setup.[50]

Regarding the direct and indirect costs of installation of the whole plants, they were calculated through a factorial approach based on the uninstalled cost of equipment and utilising similar ratio factors to those obtained *via* modelling in Aspen Plus for a plasma-based plant for nitrogen fixation.[94] Working capital was excluded from the total Capex estimation as it is expected to be recovered upon project completion.[95]

For the three analysed plants, the production capacity of 4084 kmol h^{-1} was defined based on the alternative syngas production plants based on rWGS reactors evaluated by Rezaei and Dzuryk, (2019),[77] who estimated approximate costs of $460 and $620 per tonne of syngas with H_2/CO ratios of 1 and 2, respectively. For the syngas with an H_2/CO ratio of 2, the authors used a larger capacity of 22 500 kmol h^{-1} to compare the cost with conventional SRM plants producing syngas at this ratio. Therefore, in our scenario 3, we also analysed the syngas production cost considering this larger capacity as a sensitivity analysis.

With a capacity of 4084 kmol h^{-1} and assuming an average of 8160 productive hours per year, our plants would produce 499 755 tonnes, 499 562 tonnes, and 362 622 tonnes of syngas in scenarios 1, 2, and 3, respectively. The lower production capacity in scenario 3 compared to the other scenarios is due to the higher H_2/CO ratio and the significantly lower molar mass of H_2 compared to CO.

Opex consists of variable and fixed Opex. For variable Opex, we assumed an average electricity cost of $30 per MW h for onsite generation, based on projections for onshore wind energy plants in Northern Europe in 2030.[96] The cost of CO_2 feedstock was set at $40 per tonne, reflecting the average cost used in various TEA studies for CO_2 conversion.[28,97–105] The methane feedstock cost was defined at $274 per tonne, based on a price of $5.25 per GJ.[77] The costs for high-purity deionised water and oxygen were set at $14 and $120 per tonne, respectively.[28,106,107] Cooling water costs were estimated at $0.066 per m^3, based on the method by Ulrich and Vasudevan, (2006),[108] adapted to use electricity instead of natural gas (used to produce electricity onsite) to power the cooling system.

Concerning fixed Opex, since the different plants with the same capacity have varying levels of complexity, we have set the labour cost as 5% of the total capital investment,[57,109] rather than estimating the number of operators per production capacity. The catalysts used in the WGS reactor are categorized as fixed Opex because they are replaced every four years.[82,110,111] In this regard, Chiuta *et al.*, (2016)[82] estimated that the annual maintenance of these low-temperature WGS reactors can be fixed at 10% of the total capital cost of the reactor, while the annual maintenance for the rest of the plant was fixed at 3% of the remaining total capital cost. Insurance, taxes, and licensing and permits were set at 1%, 1%, and 0.1% of the total capital investment, respectively.[109]

3. Results and discussion

3.1. Cost of production

The UCOP of syngas for the plants with a capacity of 4084 kmol h^{-1} in the three scenarios are presented in Fig. 2, and the total annual syngas production costs per item in Table 5. The syngas costs are $590, $549, and $666 per tonne in scenario 1, 2, and 3, respectively.

These results show that despite the complexity of the plants in scenarios 1 and 2, the plasma setups contribute the most to both total Capex and Opex. For syngas with an H_2/CO ratio of 1, the plasma-based conversion sections account for over 62% of the total production cost. For syngas with an H_2/CO ratio of 2, this section's contribution increases to 77% of the total cost. Moreover, despite the utilization of low-cost onsite-generated electricity, the main cost driver in these plasma sections is power consumption, except in scenario 2, where the cost of electricity is similar to the cost of CH_4 feedstock. Plasma power consumption contributes 24%, 18%, and 29% to the total UCOP of syngas in scenario 1, 2, and 3, respectively.

The high share of plasma electricity costs indicates that the most important strategy to further increase the cost-effectiveness of these alternative plasma-based syngas plants is to improve the energy efficiency of the plasma-based conversion. This is also consistent with the significant share of the plasma sections in the total Capex of the plants, as shown in Fig. 3. Analysing the Capex shares individually suggests that investing in reactor engineering development to reduce the equipment

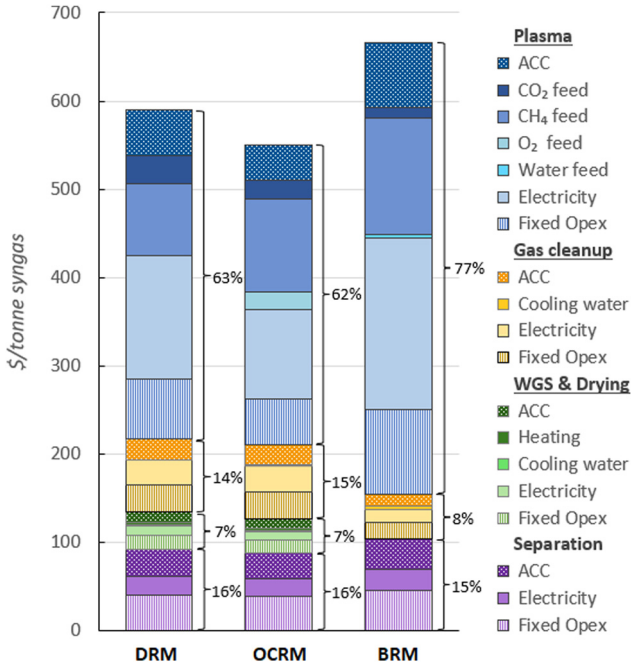

Fig. 2 Production costs of syngas with H_2/CO ratios of 1 (DRM and OCRM) and 2 (BRM) in the base cases (4084 kmol h^{-1}). The production costs are presented by section of the plants and their respective Capex and Opex. The annualised capital costs (ACC) are represented by columns with dotted patterns, fixed Opex by columns with vertical line patterns, and variable Opex by columns with solid colour patterns.

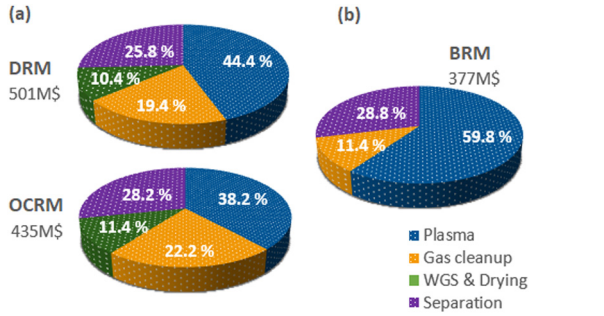

Fig. 3 Contribution of the different sections to the capital investment of the plants in the base cases. (a) Plants with a syngas H_2 : CO ratio of 1; (b) plants with a syngas H_2 : CO ratio of 2. The values under each scenario represent the total Capex (uninstalled equipment cost plus direct and indirect installation costs) in millions of dollars (M$).

cost of the plasma setup would be a relevant strategy. However, given the significant share of electricity consumption and the fact that the PSU constitutes most of the Capex for the plasma setup, any increase in the reactor's energy efficiency would automatically decrease the power required for the PSU, thereby reducing both the total Capex and fixed Opex, as well as a large part of the variable Opex.

Given the high shares of plasma equipment cost, methane feed cost, and electricity cost in the total syngas production cost, as observed in the blue-toned bars of Fig. 2 and the pie chart in Fig. 3, and the relevance of plasma power consumption (directly linked to electricity cost), we pre-selected these four parameters for a uniform sensitivity analysis. This analysis identifies the parameter with the greatest sensitivity in the syngas production cost, which is then selected for a more in-depth sensitivity analysis. In this approach, a consistent variation of ±50% was applied to the plasma power consumption and the prices of plasma equipment, methane, and electricity to evaluate their relative impact on syngas production costs, ensuring a direct comparison under

Table 5 Total annual syngas production costs per plant type in the base case (4084 kmol h^{-1}). Syngas with H_2/CO ratios of 1 (DRM and OCRM) and 2 (BRM)

		Annual syngas production costs (M$)		
Section	Item	DMR	OCRM	BRM
Plasma	Annualised capital cost (ACC)	26.13	19.50	26.46
	CO_2 feed	15.76	10.76	4.24
	CH_4 feed	40.54	52.59	47.67
	O_2 feed		10.29	
	Water feed			1.56
	Electricity	69.73	50.38	70.70
	Fixed Opex	34.56	25.85	34.47
Gas cleanup	Annualised capital cost (ACC)	11.38	11.36	5.06
	Cooling water	0.024	0.398	1.60
	Electricity	14.46	14.80	5.28
	Fixed Opex	15.05	15.06	6.59
WGS and drying	Annualised capital cost (ACC)	6.11	5.81	
	Heating	1.09	0.92	
	Cooling water	0.58	0.51	
	Electricity	5.28	4.92	
	Fixed Opex	8.08	7.70	
Separation	Annualised capital cost (ACC)	15.19	14.43	12.74
	Electricity	10.87	10.08	8.38
	Fixed Opex	20.08	19.12	16.59
TOTAL (M$)		294.94	274.49	241.35
Capacity (tonne syngas per year)		499 755	499 562	362 622
UCOP ($ per tonne syngas)		590	549	666
H_2 : CO ratio		1 : 1	1 : 1	2 : 1

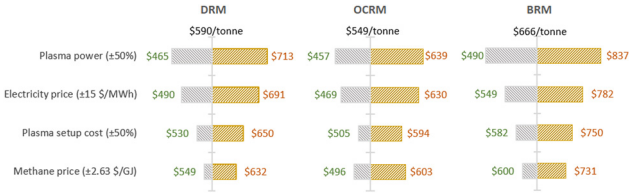

Fig. 4 Sensitivity analysis for the UCOP of syngas for each scenario in the base case. Syngas with H_2/CO ratios of 1 (DRM and OCRM) and 2 (BRM).

identical conditions. The results are presented in the tornado charts in Fig. 4.

A 50% variation in plasma power results in a UCOP variation of 21%, 17%, and 26% in scenario 1, 2, and 3, respectively, demonstrating the highest sensitivity in syngas costs to this parameter. Similarly, the impact of other parameters related to plasma power, such as the plasma setup cost and electricity price, is also significant, except in scenario 2, where the CH_4 price contributes notably to the operating expenses. Due to the more balanced cost distribution in this OCRM method, the UCOP of syngas in scenario 2 is less sensitive to variations in the cost of individual parameters compared to the other scenarios.

After observing the high sensitivity of the syngas production cost to electricity and plasma power, and considering that electricity prices are more likely to vary significantly due to market dynamics, weather events, or sociopolitical factors, we determined the need for a more in-depth sensitivity analysis of electricity prices for three scenarios.

Additionally, to benchmark our results against previous and future TEA of alternative syngas production plants, it is necessary to present the obtained UCOP using different electricity prices. For example, the referenced syngas costs from rWGS-based plants in Section 3.1 were calculated using a similar CH_4 price of \$5.25 per GJ, but with a much higher electricity price of \$70 per MW h.[77] In those rWGS-based plants, electricity represented the main expense in the syngas production cost structure. This is one reason why we did not include those syngas costs as benchmarks for our costs in Fig. 2, as it would not be a fair comparison. Furthermore, in the referenced study, neither installation costs nor fixed Opex were included in the total annual costs. Therefore, to provide a more transparent benchmark, we have updated the syngas costs reported by Rezaei and Dzuryk, (2019)[77] by estimating the installation costs and fixed Opex based on the reported total cost of bare modules and applying the ratio factors used in our study. This results in a UCOP of syngas from rWGS-based plants of \$490 and \$643 per tonne for H_2/CO ratios of 1 and 2, respectively. Therefore, parameter-specific sensitivity analyses for electricity prices for our syngas plants and the reference benchmark for each syngas ratio are presented in Fig. 5. For each scenario, a new analysis assuming a 50% reduction in the required plasma power was included.

For the production of syngas with an H_2/CO ratio of 1 (Fig. 5(a)), the plasma-based plants would have a much higher UCOP than the benchmark when electricity costs \$70 per MW h, even when considering scenarios with a 50% reduction in plasma power (dashed lines in Fig. 5(a)). If plasma power was the only variable parameter, only the plasma-based plant in scenario 2 would match the benchmark, but this would require the reactor to consume one-fifth of the base case plasma power. In contrast, producing syngas with an H_2/CO ratio of 2 in scenario 3 would be more competitive. Specifically, scenario 3 Large, using the benchmark scale of 22 500 kmol h^{-1} (equivalent to producing 2 million tonnes of syngas per year), would have a UCOP of \$436 per tonne of syngas when electricity costs \$30 per MW h. However, when electricity costs \$70 per MW h, scenario 3 Large would have a higher UCOP than the benchmark. Nevertheless, in the scenarios assuming half the plasma power consumption (series with dashed lines), both scenarios 3 (base and large) would be competitive. In detail, these reduced power cases for scenario 3 base almost matched the benchmark with a UCOP of \$649 per tonne, while scenario 3 Large had a much lower UCOP of \$505 per tonne. For scenario 3 operating at a large scale, the syngas production cost would match the benchmark if a 20% reduction in plasma power consumption were achieved, indicating that plasma-based BRM has the potential to compete with more mature electric-powered technologies such as rWGS-based plants.

Regarding the competitiveness of these electric-based alternative plants for syngas production compared to conventional fossil-based methods, such as SRM plants, the plant in scenario 3 would also be attractive. The UCOP of syngas from large SRM plants is approximately \$225 per tonne, estimated using CH_4 and electricity prices of \$5.25 per GJ and \$70 per MW h, respectively.[77] Since the electricity price is not a major cost component for these plants, their UCOP can be compared with the UCOP obtained in our scenario 3 at the same large scale, using the assumed electricity price of \$30 per MW h, which was estimated at \$436 and \$324 per tonne of syngas in the base and reduced plasma power cases, respectively, as seen in Fig. 5 (orange solid and dashed lines). In the reduced plasma power case, the plant would match this UCOP when the electricity price drops to \$10 per MW h. Therefore, given the difficulty of achieving such low electricity prices and halving plasma power consumption, improving the cost-effectiveness of these plants could also be plausible by using a less expensive CH_4 source or optimizing the syngas separation system, which also significantly impacts the plant's cost structure as observed in Fig. 4.

3.2. Life cycle assessment

3.2.1. Impact assessment. Table 6 presents the environmental impacts of the plasma-based process for syngas production under investigation, categorized by the defined midpoint impact categories, as also depicted in Fig. 6. In all three scenarios, the primary environmental impact is predominantly driven by energy demands (CEDf), accounting for approximately half of the total impacts. Freshwater ecotoxicity contributes significantly to the remaining half. The global warming potential (GWP) represents about 2.3% of the impact, while the remaining 0.04% is distributed among the other seven categories. In scenario 3, CEDf contributes the most, accounting

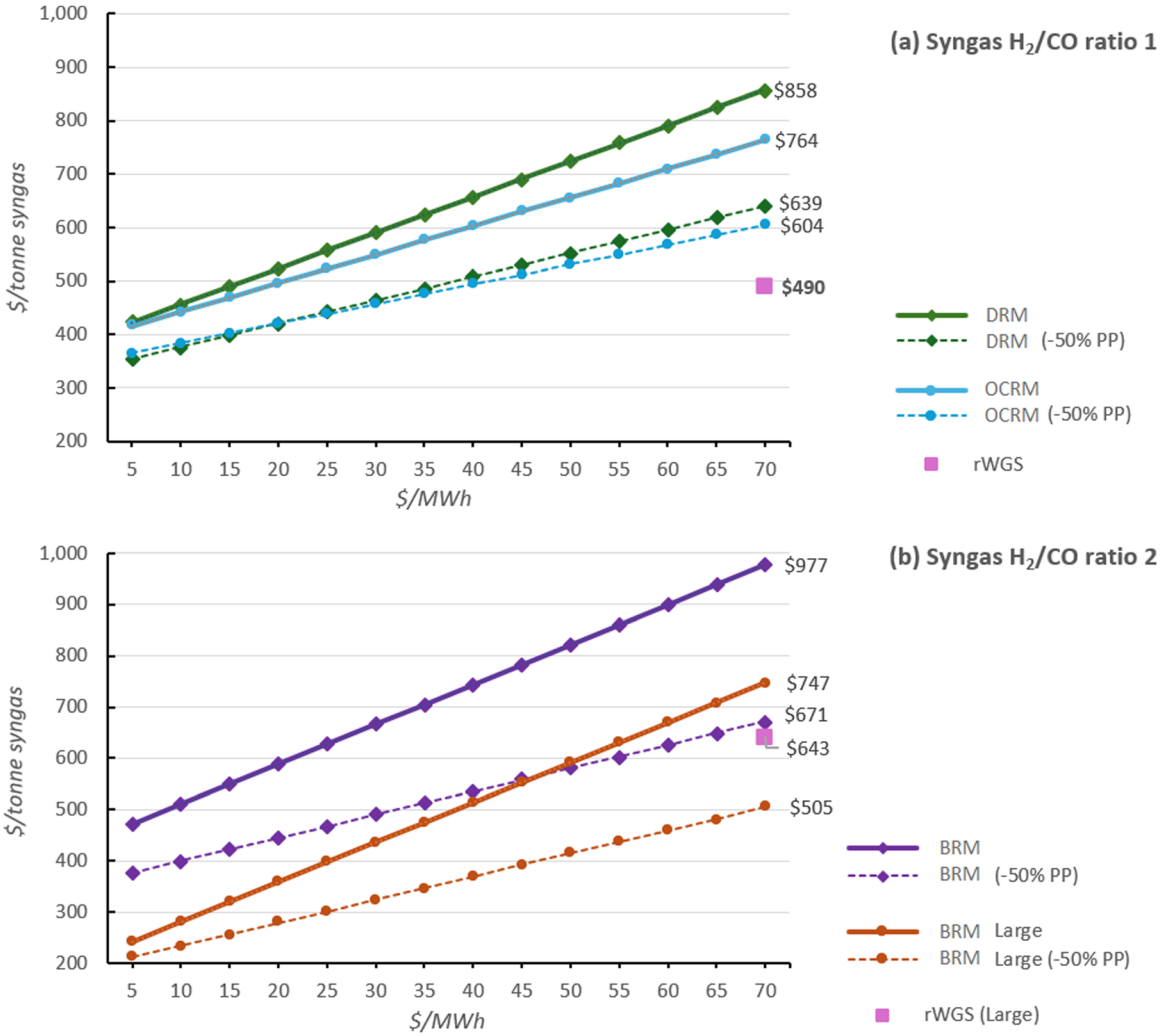

Fig. 5 Sensitivity analysis for electricity prices. Chart (a) presents scenarios 1 and 2, along with the benchmark using an rWGS-based plant to produce syngas with an H_2/CO ratio of 1. Chart (b) presents scenario 3 at base scale (4084 kmol h^{-1}), scenario 3 at large scale (22 500 kmol h^{-1}), and the benchmark using an rWGS-based plant to produce syngas with an H_2/CO ratio of 2. In both charts, new scenarios assuming a 50% reduction in plasma power (PP) are shown with dashed lines.

Table 6 Environmental impact costs per scenario in the base case (4084 kmol h^{-1})

Impact category	Units	Scenario 1 DRM	Scenario 2 OCRM	Scenario 3 BRM
Acidification	mol H^+-Eq	1.28×10^{-3}	6.88×10^{-4}	1.76×10^{-3}
Climate change	kg CO_2-Eq.	2.32×10^{1}	1.24×10^{-1}	3.10×10^{-1}
Ecotoxicity: freshwater	CTUe	5.04×10^{0}	2.47×10^{0}	5.31×10^{0}
Energy resources: non-renewable	MJ	4.81×10^{0}	2.66×10^{0}	7.06×10^{0}
Eutrophication: freshwater	kg PO_4-Eq.	1.66×10^{-4}	8.83×10^{-5}	2.21×10^{-4}
Eutrophication: terrestrial	mol N-Eq.	2.22×10^{-3}	1.16×10^{-3}	2.87×10^{-3}
Human toxicity: carcinogenic	CTUh	1.83×10^{-10}	8.79×10^{-11}	1.85×10^{-10}
Human toxicity: non-carcinogenic	CTUh	5.24×10^{-9}	2.50×10^{-9}	4.89×10^{-9}
Material resources: metals/minerals	kg Sb-Eq.	1.38×10^{-5}	6.02×10^{-6}	1.04×10^{-5}
Photochemical ozone formation: human health	kg NMVOC-.	6.36×10^{-4}	3.46×10^{-4}	8.99×10^{-4}

for 55%. In contrast, in scenario 1, CEDf contributes the least, at 47.7%, with scenario 2 falling in between. This distribution of contributions is inversely related to FET (50 and 42% for scenarios 1 and 3 respectively), as the variation in GWP lies within a narrow range of 2.29% to 2.45%. These results confirm the high energy dependency of plasma-mediated technology. In this context, the final mixture is intended for commercial storage, rather than emission and consequently not considered

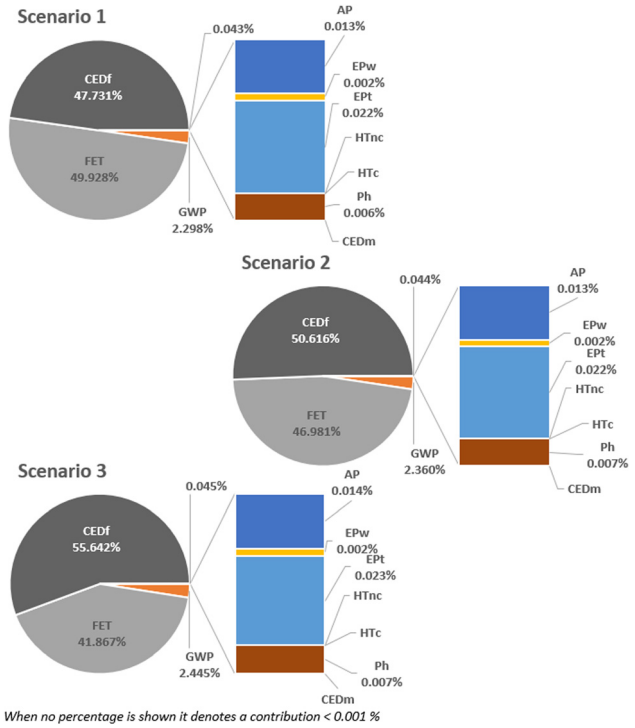

Fig. 6 Contribution of the different impact categories to the global impacts according to the defined scenarios.

as emissions. Whilst at the inlet of the process in scenario 1, 83% of the consumed gases are CO_2 and 16% CH_4, at the outlet the composition shifts significantly, with CO and H_2 comprising 49% and 51%, respectively, so that the emissions of CH_4 and CO_2 are reduced to less than 0.2%. Approximately 10% of the initial mass is converted into secondary gases, including H_2O vapor, C_2H_4, C_2H_2, and C_2H_6. The latter three gases are condensed during the second gas cleanup step using PSA, while water is removed in the fourth step through cryogenic drying. For the purpose of this study, all of these gases have been considered as by-products, together with 1% production loses considered along the process, and therefore classified as waste, despite their potential suitability as raw materials for secondary processes. In the dual PSA system, a portion of the flow stream is recycled, containing 0.81 g min^{-1} of CO_2, 0.0068 g min^{-1} of CH_4, and 0.001 g min^{-1} of CO. These components are not regarded as waste because they are reintroduced into the process. In scenario 2, the CO_2 concentration in the inlet is reduced to 67%, while the CH_4 concentration is increased to 24%. To achieve the same syngas composition as in scenario 1, an additional 9% O_2 is required, leaving other emissions below 0.2%. Scenario 3 involves the addition of 40% water, resulting in a significant difference compared to the other two scenarios. In this case, CO_2 constitutes only 29% of the inlet composition, while CH_4 accounts for 31%. This leads to an immediate increase in the recycling flow stream, with 50% of the unreacted CO_2, 25% of the initial CH_4, and 62% of the H_2O being recycled. Additionally, the introduction of water also leads to increased waste generation. The outlet composition in scenario 3 includes 66% H_2 and 34% CO, with CH_4 and CO_2 levels reduced to below 0.2%.

The environmental categories are calculated from mass and energy flow data, which, while being experimental, are highly certain due to the high standard of modern process control of chemical plants. Moreover, we use the environmental impact data from LCA databases, which are also without uncertainty. Uncertainty exists for the yield of the plasma reactions. They can vary somewhat for diverse experiments. The environmental impact categories were calculated by considering a ±20% variation in yield for each scenario. This resulted in average impact differences of ±5% for scenario 1, ±9.5% for scenario 2, and ±17.4% for scenario 3. Since energy expenses remained constant in this assessment, we conclude that scenario 3 is more sensitive to fluctuations in process yield, whereas scenario 1 is more robust to processing variations, indicating a greater dominance of energy expenses in the latter. Another source of uncertainty can be the quality of the feed material. This is not an issue for the fossil natural gas, which is industrially refined to 100% methane, yet it is an issue for biomethane, which is a prominent source for future plasma operations. Biomethane has a variable content of methane depending on the source, with estimates ranging from 50% to 75% in different scenarios.[112] Nevertheless, the influence of switching to biomethane was negligible, as the variation remained below 0.01% in all scenarios.

3.2.2. Sensitivity assessment. For the study presented here, the low-voltage European energy mix was used from the Ecoinvent database to quantify the associated impacts. However, these impacts could be mitigated by adopting an optimal renewable energy mix. In this context, Heide *et al.* described an optimal mix for a fully renewable energy scenario in Europe,[113] recommending a seasonal mix of 55% wind and 45% solar power generation. In scenarios with less than 100% renewable energy, the proportion of wind power increases, while that of solar power decreases. Yet, in this study the ideal scenario of 100% renewable energy was considered as a sensitivity analysis and the decrease in impact categories was evaluated using data obtained from Ecoinvent, as depicted in Fig. 7. Transitioning from non-renewable to renewable energy sources would substantially reduce environmental impacts of the whole process. The categories CEDf and EPw would result in more than an 80% reduction in impacts, while GWP and EPt would reduce impacts by over 70% and 65%, respectively. Together, these four categories account for more than 99% of the environmental impacts in the global LCA presented in this work. On the other side, the exclusive use of renewable energy sources would result in a modest increase in environmental impacts concerning acidification potential (AP) and carcinogenic human toxicity (HTc), although these increases would be less than 1%.

3.2.3. Benchmarking assessment. Fig. 8 and 9 illustrate the comparison between scenarios 2 and 3 relative to scenario 1. The data are normalized to a value of one, where values in the range (0,1) indicate reduced impacts compared to scenario 1, and values greater than one indicate increased impacts.

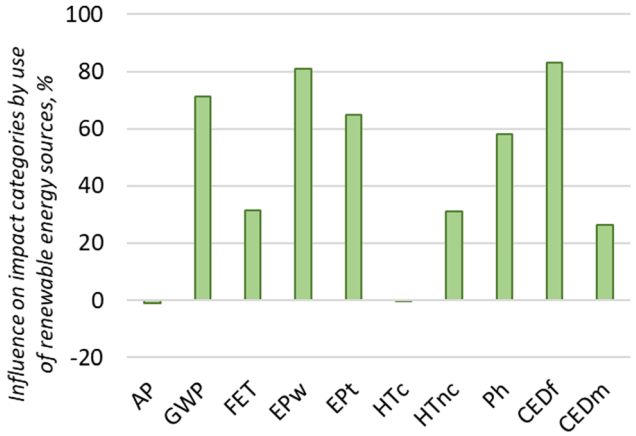

Fig. 7 Influence on environmental impact categories in the case of the substitution of the current European energy source by a fully optimized renewable energy source.

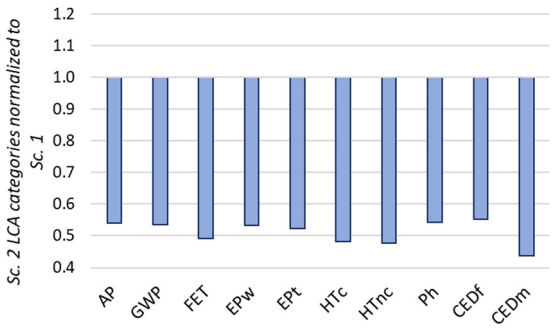

Fig. 8 Comparison of environmental impact categories with scenario 2 normalized to scenario 1 (*a* value of 1 means the same value in scenario 2 and in scenario 1).

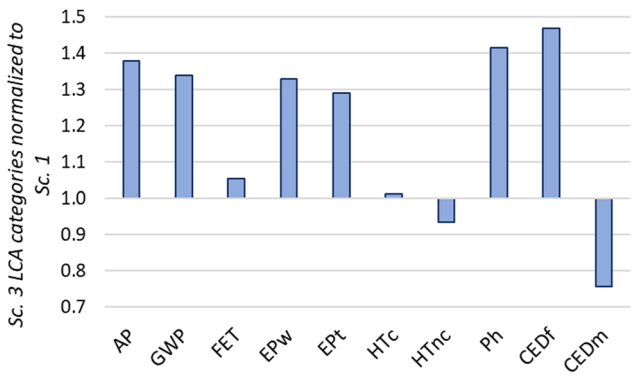

Fig. 9 Comparison of environmental impact categories with scenario 3 normalized to scenario 1 (*a* value of 1 means the same value in scenario 2 and in scenario 1).

The figures clearly show opposing trends: Scenario 2 demonstrates improvements over scenario 1 across all impact categories by approximately 50%, while scenario 3 exhibits increased environmental impacts in 8 out of 10 categories, with the exceptions being HTnc and CEDm. Key environmental impact categories, such as EPw and GWP, which contribute

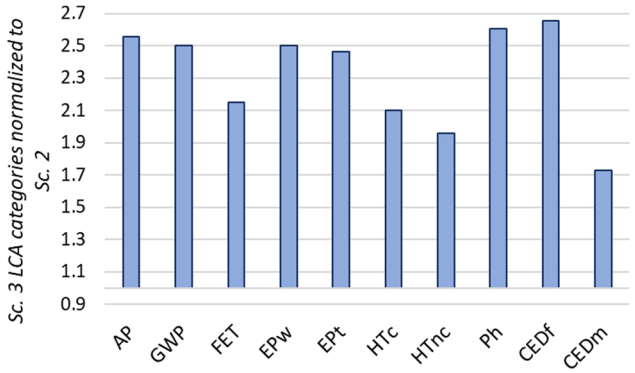

Fig. 10 Comparison of environmental impact categories with scenario 3 normalized to scenario 2 (*a* value of 1 means the same value in scenario 2 and in scenario 1).

significantly to the overall environmental footprint of the process, have shown an increase in impacts by approximately 30%. Additionally, energy consumption (CEDf) rises by around 45%.

Based on the environmental impact results, scenario 3 exhibits the highest impacts, whereas scenario 2 has the lowest. This contrast is clearly illustrated in Fig. 10, where the environmental impacts of scenario 3 (the highest) are more than twice in 8 over 10 categories of scenario 2 (the lowest). The significant difference is primarily due to the additional water usage and increased energy requirements associated with scenario 3. Consequently, we conclude that OCRM (scenario 2) is the best choice from an environmental point of view, while BRM (scenario 3) exhibits the highest environmental impacts.

Following the evaluation of the environmental performance of plasma-based syngas production from CH_4-rich natural gas across three scenarios, *i.e.*, DRM (scenario 1), OCRM (scenario 2) and BRM (scenario 3), we now compare the results with the existing state-of-the-art SRM technology using the cradle-to-gate LCA. For benchmarking our alternatives against the current leading technology, the literature report by Matin and Flanagan (2024)[114] was used. In the referenced literature, the authors employed the TRACI methodology to quantify environmental impacts, which offers characterization factors for LCA particularly applicable to processes, products, facilities, companies, and communities. However, this methodology is primarily tailored for use within the United States. In this case the impact categories are acidification potential (AP – moles H^+-eq.), carcinogenics (HTc – Kg benzene-eq.), ecotoxicity (ET – kg 2.4-D-eq.), eutrophication (EP – kg N-eq.), fossil fuel depletion (CEDf – MJ), global warming potential (GWP – kg CO_2-eq.), non-carcinogenics (HTnc – kg toluene-eq.), ozone depletion potential (OD – kg CFC-11-eq.) and respiratory effects (RE – kg PM2.5-eq.). Since our initial assessment was conducted using the EF3.1 framework, closer to and recommended by European institutions, it was necessary to recalculate our data using TRACI to enable meaningful benchmarking. We needed to use conversion parameters as described by Thiel *et al.* (2015)[115] to ensure appropriate use of units. Additionally, the

Table 7 Benchmarking of LCA values compared with data obtained from ref. 114 (DBD = dielectric barrier discharge, SRM = steam reforming of methane, NTP = non thermal plasma, A–G different allocations) (impact categories acidification potential (AP-kgSO_2-eq.), carcinogenics (HTc-CTUh), ecotoxicity (ET-CTUe), eutrophication (EP-kg N-eq.), fossil fuel depletion (CEDf-MJ), global warming potential (GWP-kg CO_2-eq.), non-carcinogenics (HTnc-CTUh), ozone depletion potential (OD-kg CFC-11-eq) and respiratory effects (RE-kg PM2.5-eq.))

	Literature reference								Our work		
	SRM-A	SRM-B	SRM-C	SRM-C-DBD	NTP-DRM-D	NTP-DRM-E	NTP-DRM-F	NTP-DRM-G	NTP-DRM Scenario 1	NTP-OCRM Scenario 2	NTP-BRM Scenario 3
GWP	8.41×10^{0}	9.60×10^{0}	1.05×10^{1}	1.81×10^{1}	1.46×10^{2}	8.83×10^{1}	2.05×10^{1}	2.39×10^{1}	5.98×10^{-1}	3.18×10^{-1}	8.03×10^{-1}
EP	9.60×10^{-3}	1.10×10^{-2}	1.10×10^{-2}	1.18×10^{-2}	6.42×10^{-2}	3.88×10^{-2}	1.27×10^{-2}	1.29×10^{-2}	7.20×10^{-5}	3.96×10^{-5}	9.77×10^{-5}
AP	3.04×10^{-2}	3.38×10^{-2}	5.90×10^{-2}	3.69×10^{-2}	2.53×10^{-1}	1.52×10^{-1}	4.47×10^{-2}	4.76×10^{-2}	6.40×10^{0}	3.39×10^{0}	8.51×10^{0}
OD	1.88×10^{-6}	2.00×10^{-6}	1.95×10^{-6}	2.03×10^{-6}	2.40×10^{-5}	1.45×10^{-5}	4.50×10^{-6}	4.70×10^{-6}	1.65×10^{-8}	9.69×10^{-9}	2.28×10^{-8}
ET	2.08×10^{1}	2.25×10^{1}	2.23×10^{1}	2.48×10^{1}	1.53×10^{2}	9.21×10^{1}	3.43×10^{1}	3.36×10^{1}	2.74×10^{2}	1.38×10^{2}	3.20×10^{2}
RE	3.95×10^{-3}	4.41×10^{-3}	5.85×10^{-3}	4.70×10^{-3}	2.77×10^{-2}	1.67×10^{-2}	5.66×10^{-3}	5.74×10^{-3}	1.42×10^{-3}	7.55×10^{-4}	1.91×10^{-3}
HTC	1.94×10^{7}	2.08×10^{7}	2.10×10^{7}	2.33×10^{7}	1.32×10^{-6}	7.93×10^{7}	3.26×10^{7}	3.11×10^{7}	6.79×10^{-10}	3.15×10^{-10}	6.21×10^{-10}
HTnc	9.71×10^{7}	1.09×10^{-6}	1.24×10^{-6}	1.33×10^{-6}	8.81×10^{-6}	5.31×10^{-6}	1.45×10^{-6}	1.58×10^{-6}	1.59×10^{7}	7.61×10^{-8}	1.60×10^{7}
CEDf	3.84×10^{1}	4.04×10^{1}	3.85×10^{1}	3.95×10^{1}	4.37×10^{2}	2.64×10^{2}	8.83×10^{1}	9.00×10^{1}	4.81×10^{0}	2.66×10^{0}	7.06×10^{0}

Fig. 11 Orders of magnitude differences on environmental impacts between literature references and our work.

process was proportionally scaled to match the same functional unit used in this study. However, the impact categories of acidification, carcinogenics, non-carcinogenics, and ecotoxicity required alignment with the process LCA, needing some additional unit conversions. To this aim, we used the factors proposed by Thiel *et al.* (2015),[115] namely: for acidification potential, a characterization factor of 50.79 kg SO_2 equivalent per mole H^+ was used. The economic input–output life-cycle assessment (EIO-LCA) method reports human health toxicity impacts (both cancerous and non-cancerous) in terms of benzene and toluene equivalent emissions into air. Consequently, TRACI characterization factors of 2.97×10^{-7} CTUh per kg of benzene into air and 5.3×10^{-8} CTUh per kg of toluene into air were utilized, where CTUh represents the cumulative toxicity unit for humans. Ecotoxicity, as reported by EIO-LCA, is expressed as kg 2,4-DCB to continental freshwater, and a characterization factor of 8.60×10^{2} CTUe per kg 2,4-DCB was employed, with CTUe denoting the cumulative toxicity unit for the environment. It is important to note that the EIO-LCA analysis did not account for the fate of chemicals in soil and water concerning human toxicity, nor in air and soil for ecotoxicity. Matin and Flanagan, (2024)[114] evaluated the environmental impacts of plasma-based DRM methods relative to traditional thermal SRM by employing eight different allocation scenarios. The corresponding values for these allocations were also included in this study to provide additional comparative sources. The comparative results of the data gathered from the literature, after scaling and unit homogenization, are presented in Table 7. There are significant differences between the values reported in the literature and the results obtained in our study. These discrepancies may stem from variations in allocation methods or differing assumptions made during the process design. These differences span several orders of magnitude, either in favour or against. To address this issue, the orders of magnitude were analysed as shown in Fig. 11.

Accordingly, values above zero indicate that our process improved the reported outcomes when compared to the literature, whereas values below zero denote our process increased environmental impacts by the same magnitude. As shown, most impact categories benefited from our process, with values exceeding zero in 7 over 9 impact categories assessed. Notably, OD, HTc, and EP demonstrated improvements exceeding 2

Table 8 Overall circularity calculations of MCI and other partial indicators according to EMAF methodology, for each scenario

Symbol	Definition	Scenario 1 (DRM)	Scenario 2 (OCRM)	Scenario 3 (BRM)
M	Mass of raw materials	2.51	2.18	2.04
F_R	Fraction of mass from recycled sources	0.53	0.49	0.47
V	Materials not from reuse	1.18	1.11	1.08
W	Mass of unrecoverable waste	0.078	0.076	0.113
W_0	Mass of unrecoverable waste through emissions	0.052	0.050	0.073
W_F	Mass of unrecoverable waste generated when producing recycled feedstock	0.054	0.052	0.079
LFI	Linear flow index (material flowing in a linear fashion)	0.250	0.270	0.290
MCI	Material circularity indicator	0.775	0.757	0.739

orders of magnitude. On the counterpart, AP and ET yielded values below zero, indicating increased environmental impacts from the plasma-based process scenarios presented here. Regarding critical environmental impacts, namely ET and CEDf, the results present opposite conclusions. On one hand, environmental impacts related to energy consumption were reduced by 1.4 orders of magnitude, while on the other hand, our process increased ecotoxicity by 0.7 orders of magnitude. This increase may be due to secondary compounds generated during the process. Appropriate capture of these compounds could potentially reduce emissions and thus mitigate ET.

3.3. Circularity metrics of the process

This study was performed using the material flow data presented in the process inventories (Tables 2 and 3), as well as the following assumptions (Table 8): (i) 1% losses along the process, (ii) utility factor was not considered as the obtained syngas was considered to have the same purity in all cases and the same lifetime depending on the demand, (iii) the recycling efficiency was considered the same in all scenarios and therefore non-significant for benchmarking, and (iv) the unreacted CO_2, CO and CH_4 are appropriately separated and recycled to the inlet stream. The calculation of circular indices includes the global mass of inputs (M), including the flow stream (F_R) coming from the recycling loop, which at the same time defines the quantity of new raw materials (V). One key circular metric is the waste generations (including unrecoverable mass fraction (W) and waste generated when recycling (W_F)), which are assessed using the EMAF methodology, resulting in a linear flow index (LFI). The material circularity indicator (MCI) is directly calculated as a function of LFI, reflecting the process's circularity ranging from 0 (fully linear) to 1 (fully circular).

The circularity of the three scenarios is assessed as medium-high, with the first scenario achieving the highest score (0.775) and the third scenario the lowest (0.739). The scenarios exhibit similar circularity in terms of mass flows, as indicated by the narrow range of material circularity indicator (MCI) values, all within 0.036. The comparatively lower circularity of scenario 3 (BRM) is primarily attributed to a 48% increase in waste generation and an 11% reduction in recycling flow streams. Scenario 1 (DRM), which attains the highest MCI of 0.775, is characterized by a higher recycling rate and moderate waste production relative to the other scenarios.

While there are no quantitative circularity statements regarding syngas in the literature, a few papers provide solid qualitative insights into its circularity potential. Bachmann *et al.*, (2023)[116] highlighted the importance of alternative syngas pathways in reducing greenhouse gas emissions but emphasize the need for consistent assessments across studies. Frantzi and Zabaniotou, (2021)[117] proposed a circular economy model for syngas production from waste biomass but focus on process conceptualization rather than quantifiable circularity metrics. Similarly, Nisamaneenate *et al.*, (2024)[118] discussed syngas production *via* steam reforming of petroleum sludge, linking it to circular fuel production, but again without presenting direct circularity calculations. To extend our benchmark assessment, we also considered related processes, such as hydrogen production from biogas reforming. In this case, Hajjaji *et al.*, (2016)[119] conducted an LCA of the process, reporting an equivalent carbon footprint of 0.72 kg CO_2-eq per kg H_2. Additionally, Bachmann *et al.*, (2023)[116] analysed syngas production from biomass, CO_2, and steel mill off-gas, reporting a carbon footprint of 0.05 kg CO_2-eq per kg syngas for dry reforming. Using this latter value as a reference, the plasma-based process herewith reported results in a fourfold increase in carbon footprint. In contrast, when compared with biogas-derived hydrogen, the increase is by a factor of 14. As a result, the plasma process leads to a 66% reduction in carbon footprint. Anyway, all processes considered gave a carbon footprint in the same order of magnitude.

4. Conclusions

This study fills the gap of the lack of studies about the environmental impacts associated with the use of plasma-assisted CH_4 reforming processes for syngas production. We conducted a comprehensive TEA, encompassing all three scenarios, along with their respective sub-scenarios. This analysis was designed to evaluate varying market price conditions in detail, which were highly influenced by the production scale. Scenario 3 (BRM), which exhibited the highest UCOP, changed from an initial $649, reducing 20% when operating at large scale, denoting a highly competitive capacity in the near future when compared with electric-powered technologies such as rWGS-based plants. Overall, the production capacity in scenarios 1 (DRM) and 2 (OCRM) were around 500 kt syngas per year, while scenario 3 (BRM) exhibited a lower productivity of 363 kt per year. Nonetheless, under the assumption of the production cost in scenario 3 (BRM), this scenario achieved the highest rank,

attaining a score of 666 $ per t syngas, which was 13% and 21% higher when compared with scenarios 1 (DRM) and 2 (OCRM), respectively, concluding in a lower productivity at higher costs for scenario 3 (BRM). Scenario 2 (OCRM) resulted in being the most competitive in terms of high productivity, 499.6 kt per year at lower cost, *i.e.*, 549 $ per t syngas.

To evaluate the environmental impact of the process, we performed a prospective cradle-to-gate life cycle assessment comparing all three scenarios, and an external benchmarking with the current state-of-the-art SRM for H_2 production, which included additionally microwave (NTP-DRM-G) and pulsed plasma discharges (NTP-DRM-F). The energy expenses (47–55%) and eutrophication potential (41–49%) accounted for most of the environmental impacts in all scenarios, with scenario 2 (OCRM) being the most advantageous in an environmental perspective, followed by scenario 1 (DRM) and scenario 3 (BRM). When benchmarking with other syngas production processes, our process exhibited better performance in 7 over 9 environmental categories, denoting a significant improvement with respect to the current state-of-the-art SRM technologies. Given the energy-intensive nature of plasma-based DRM processes and excluding the use of renewable energy sources, the potential for improving the environmental performance of plasma-based DRM is strongly influenced by the energy consumption per unit mass of syngas produced. Therefore, future research should prioritize optimizing plasma power consumption by refining discharge parameters and improving energy efficiency.

This study directly supports 3 of the UN global sustainability goals, particularly SDG 7 (Affordable and Clean Energy), SDG 9 (Industry, Innovation, and Infrastructure), and SDG 13 (Climate Action). The transition towards renewable energy sources for plasma-assisted reforming presents a viable pathway for reducing the carbon footprint of syngas production. In the context of circularity, scenario 1 (DRM) exhibited the highest material circularity indicator (MCI) value, reaching 0.775. This was followed by scenario 2 (OCRM), which had slightly lower MCI (0.757), and scenario 3 (BRM) (0.739), which had the lowest MCI among the three scenarios, due to the lower recycling stream capacity and the higher waste production. Plasma-assisted reforming technologies generally align with global sustainability goals by addressing key challenges in clean energy (SDG 7), climate action (SDG 13), and sustainable industrial practices (SDG 12), due to using renewable energies and abundant feed sources (*e.g.* air). By demonstrating improved environmental performance and promoting material circularity, these processes contribute to industrial innovation and infrastructure (SDG 9).

Author contributions

M. Escriba-Gelonch: writing – original draft, visualization, investigation, conceptualization, methodology. J. Osorio-Tejada: writing – original draft, visualization, investigation, conceptualization, methodology. L. Yu: Process definition. B. Wanten: visualization, investigation, writing. A. Bogaerts: writing – reviewing and editing, supervision. V. Hessel: writing – reviewing and editing, supervision.

Data availability

Data for this article, will be available at the open repository at **https://repositori.udl.cat/**. This paper will be eligible to benefit from the Read and Publish agreement with Universitat de Lleida.

Conflicts of interest

There are no conflicts to declare.

Acknowledgements

We gratefully acknowledge financial support by the European Research Council (ERC) under the European Union's Horizon 2020 research and innovation programme (grant agreement no. 810182-SCOPE ERC Synergy project).

Notes and references

1 X. Li, D. Li, H. Tian, L. Zeng, Z. J. Zhao and J. Gong, *Appl. Catal., B*, 2017, **202**, 683–694.
2 IEA, CO_2 Emissions in 2023, Paris, 2024.
3 C. Wang, Y. Wang, M. Chen, D. Liang, Z. Yang, W. Cheng, Z. Tang, J. Wang and H. Zhang, *Int. J. Hydrogen Energy*, 2021, **46**, 5852–5874.
4 H. Zhang, D. Kaczmarek, C. Rudolph, S. Schmitt, N. Gaiser, P. Obwald, T. Bierkandt, T. Kasper, B. Atakan and K. Kohse-Höinghaus, *Combust. Flame*, 2022, **237**, 111863.
5 A. Paykani, H. Chehrmonavari, A. Tsolakis, T. Alger, W. F. Northrop and R. D. Reitz, *Prog. Energy Combust. Sci.*, 2022, **90**, 100995.
6 N. A. K. Aramouni, J. G. Touma, B. A. Tarboush, J. Zeaiter and M. N. Ahmad, *Renewable Sustainable Energy Rev.*, 2018, **82**, 2570–2585.
7 T. V. Choudhary and V. R. Choudhary, *Angew. Chem., Int. Ed.*, 2008, **47**, 1828–1847.
8 W. Lu, Q. Cao, B. Xu, H. Adidharma, K. Gasem, M. Argyle, F. Zhang, Y. Zhang and M. Fan, *J. Cleaner Prod.*, 2020, **265**, 121786.
9 Z. Li and K. Sibudjing, *ChemCatChem*, 2018, **10**, 2994–3001.
10 B. Abdullah, N. A. Abd Ghani and D.-V. N. Vo, *J. Cleaner Prod.*, 2017, **162**, 170–185.
11 D. Pakhare and J. Spivey, *Chem. Soc. Rev.*, 2014, **43**, 7813–7837.
12 A. Al-Fatesh, S. K. Singh, G. S. Kanade, H. Atia, A. H. Fakeeha, A. A. Ibrahim, A. M. El-Toni and N. K. Labhasetwar, *Int. J. Hydrogen Energy*, 2018, **43**, 12069–12080.
13 A. M. Ranjekar and G. D. Yadav, *J. Indian Chem. Soc.*, 2021, **98**, 100002.
14 C. Mateos-Pedrero, S. R. G. Carrazán, R. M. Blanco and P. Ruíz, *Catal. Today*, 2010, **149**, 254–259.

15 U. Oemar, K. Hidajat and S. Kawi, *Int. J. Hydrogen Energy*, 2015, **40**, 12227–12238.
16 V. R. Choudhary, K. C. Mondal and T. V. Choudhary, *Fuel*, 2006, **85**, 2484–2488.
17 J. R. Rostrup-Nielsen, *Catal. Today*, 2002, **71**, 243–247.
18 N. Kumar, M. Shojaee and J. J. Spivey, *Curr. Opin. Chem. Eng.*, 2015, **9**, 8–15.
19 D. He, Y. Zhang, Z. Wang, Y. Mei and Y. Jiang, *Energy Fuels*, 2020, **34**, 4822–4827.
20 A. Nakhaei Pour and M. Mousavi, *Int. J. Hydrogen Energy*, 2015, **40**, 12985–12992.
21 U. S. Mohanty, M. Ali, M. R. Azhar, A. Al-Yaseri, A. Keshavarz and S. Iglauer, *Int. J. Hydrogen Energy*, 2021, **46**, 32809–32845.
22 M. E. E. Abashar, *Int. J. Hydrogen Energy*, 2004, **29**, 799–808.
23 R. R. Ikreedeegh and M. Tahir, *Fuel*, 2021, **305**, 121558.
24 B. King, D. Patel, J. Zhu Chen, D. Drapanauskaite, R. Handler, T. Nozaki and J. Baltrusaitis, *Fuel*, 2021, **304**, 121328.
25 E. Delikonstantis, M. Scapinello and G. D. Stefanidis, *Energies*, 2017, **10**, 1429.
26 S.-A. Theofanidis, K. Stergiou, E. Delikonstantis and G. D. Stefanidis, *Ind. Eng. Chem. Res.*, 2024, **63**, 12035–12052.
27 H. Lamberts-Van Assche, G. Thomassen and T. Compernolle, *J. CO_2 Util.*, 2022, **64**, 102156.
28 J. Osorio-Tejada, M. Escriba-Gelonch, R. Vertongen, A. Bogaerts and V. Hessel, *Energy Environ. Sci.*, 2024, **17**, 5745–6128.
29 N. Budhraja, A. Pal and R. S. Mishra, *Int. J. Hydrogen Energy*, 2023, **48**, 2467–2482.
30 K. Wang, X. Ren, G. Yin, E. Hu and H. Zhang, *Curr. Opin. Green Sustainable Chem.*, 2024, **50**, 100981.
31 J. Feng, X. Sun, Z. Li, X. Hao, M. Fan, P. Ning and K. Li, *Adv. Sci.*, 2022, **9**, 2203221.
32 L. Tang, H. Huang, H. Hao and K. Zhao, *J. Electrost.*, 2013, **71**, 839–847.
33 S. M. A. Mousavi, W. Piavis and S. Turn, *Fuel Process. Technol.*, 2019, **193**, 378–391.
34 H. Chen, Y. Mu, S. Xu, S. Xu, C. Hardacre and X. Fan, *Chin. J. Chem. Eng.*, 2020, **28**, 2010–2021.
35 W.-C. Chung and M.-B. Chang, *Renewable Sustainable Energy Rev.*, 2016, **62**, 13–31.
36 A. Bogaerts and E. Neyts, *ACS Energy Lett.*, 2018, **3**, 1013–1027.
37 R. Snoeckx and A. Bogaerts, *Chem. Soc. Rev.*, 2017, **46**, 5805–5863.
38 B. Wanten, S. Maerivoet, C. Vantomme, J. Slaets, G. Trenchev and A. Bogaerts, *J. CO_2 Util.*, 2022, **56**, 101869.
39 Y. Pang, H. Bosch, T. Hammer, D. Müller and J. Karl, *Waste Biomass Valorization*, 2020, **11**, 675–688.
40 M. Ramakers, G. Trenchev, S. Heijkers, W. Wang and A. Bogaerts, *ChemSusChem*, 2017, **10**, 2642–2652.
41 R. Vertongen and A. Bogaerts, *J. CO_2 Util.*, 2023, **72**, 102510.
42 J. C. Whitehead, *J. Phys. D:Appl. Phys.*, 2016, **49**, 243001.
43 M. Scapinello, E. Delikonstantis and G. D. Stefanidis, *Chem. Eng. Process.*, 2017, **117**, 120–140.
44 V. Maslova, R. Nastase, G. Veryasov, N. Nesterenko, E. Fourré and C. Batiot-Dupeyrat, *Prog. Energy Combust. Sci.*, 2024, **101**, 101096.
45 B. Wanten, Y. Gorbanev and A. Bogaerts, *Fuel*, 2024, **374**, 132355.
46 S. Maerivoet, B. Wanten, R. De Meyer, M. Van Hove, S. Van Alphen and A. Bogaerts, *ACS Sustainable Chem. Eng.*, 2024, **12**, 11419–11434.
47 M. Escribà-Gelonch, J. Bricout and V. Hessel, *ACS Sustainable Chem. Eng.*, 2021, **9**, 1867–1879.
48 M. Escribà-Gelonch, J. Osorio-Tejada, R. Vertongen, A. Bogaerts and V. Hessel, *J. Cleaner Prod.*, 2025, **488**, 144578.
49 V. Hessel, M. Escribà-Gelonch, J. Bricout, N. N. Tran, A. Anastasopoulou, F. Ferlin, F. Valentini, D. Lanari and L. Vaccaro, *ACS Sustainable Chem. Eng.*, 2021, **9**, 9508–9540.
50 C. O'Modhrain, G. Trenchev, Y. Gorbanev and A. Bogaerts, *ACS Eng. Au*, 2024, **3**, 333–344.
51 M. Escribà-Gelonch, G. A. de Leon Izeppi, D. Kirschneck and V. Hessel, *ACS Sustainable Chem. Eng.*, 2019, **7**, 17237–17251.
52 R. Schenk, V. Hessel, C. Hofmann, J. Kiss, H. Löwe and A. Ziogas, *Chem. Eng. J.*, 2004, **101**, 421–429.
53 T. Ombrello, X. Qin, Y. Ju, A. Gutsol and A. Fridman, in 43rd AIAA Aerospace Sciences Meeting and Exhibit, American Institute of Aeronautics and Astronautics, 2005.
54 D. Staack, B. Farouk, A. Gutsol and A. Fridman, *Plasma Sources Sci. Technol.*, 2005, **14**, 700.
55 L. Ai, S.-F. Ng and W.-J. Ong, *ChemSusChem*, 2022, **15**, e202201700.
56 G. Z. S. Ling, J. J. Foo, X.-Q. Tan and W.-J. Ong, *ACS Sustainable Chem. Eng.*, 2023, **11**, 5547–5558.
57 C. Choe, S. Cheon, J. Gu and H. Lim, *Renewable Sustainable Energy Rev.*, 2022, **161**, 112398.
58 A. Sternberg and A. Bardow, *ACS Sustainable Chem. Eng.*, 2016, **4**, 4156–4165.
59 M. Puig-Gamero, M. M. Parascanu, P. Sánchez and L. Sanchez-Silva, *Environ. Sci. Pollut. Res.*, 2021, **28**, 30335–30350.
60 G. Li, S. Ma, F. Liu, X. Zhou, K. Wang and Y. Zhang, *Bioresour. Technol.*, 2021, **342**, 125940.
61 F. Ardolino and U. Arena, *Waste Manage.*, 2019, **87**, 441–453.
62 H. J. Oh, J. K. Ko, G. Gong, S.-M. Lee and Y. Um, *Front. Bioeng. Biotechnol*.
63 N. Schiaroli, M. Volanti, A. Crimaldi, F. Passarini, A. Vaccari, G. Fornasari, S. Copelli, F. Florit and C. Lucarelli, *Energy Fuels*, 2021, **35**, 4224–4236.
64 GVR, Grand View Research, **https://www.grandviewresearch.com/industry-analysis/syngas-market-report**, (accessed 28 February 2025).
65 M. Farsi, Advances in Synthesis Gas: Methods, Technologies and Applications, *Syngas Process Modelling and Apparatus Simulation*, 2023, vol. 4, pp. 381–399.
66 G. Bozzano and F. Manenti, *Prog. Energy Combust. Sci.*, 2016, **56**, 71–105.

67 J. Osorio-Tejada, K. van't Veer, N. V. D. Long, N. N. Tran, L. Fulcheri, B. S. Patil, A. Bogaerts and V. Hessel, *Energy Convers. Manage.*, 2022, **269**, 116095.
68 W. Aich, K. A. Hammoodi, L. Mostafa, M. Saraswat, A. Shawabkeh, D. J. jasim, L. Ben Said, A. S. El-Shafay and A. Mahdavi, *Process Saf. Environ. Prot.*, 2024, **184**, 1158–1176.
69 N. S. Matin and W. P. Flanagan, *Int. J. Hydrogen Energy*, 2024, **49**, 1405–1413.
70 B. Wanten, R. Vertongen, R. De Meyer and A. Bogaerts, *J. Energy Chem.*, 2023, **86**, 180–196.
71 G. Trenchev, A. Nikiforov, W. Wang, S. Kolev and A. Bogaerts, *Chem. Eng. J.*, 2019, **362**, 830–841.
72 S. Renninger, M. Lambarth and K. P. Birke, *J. CO_2 Util.*, 2020, **42**, 101322.
73 E. Hughes, in *Electrical and Electronic Technology*, ed. J. Hiley, K. Brown, I. McKenzie Smith, Pearson Education Limited, 10th edn, 2008.
74 G. Towler and R. Sinnott, Chemical Engineering Design: Principles, in *Practice and Economics of Plant and Process Design*, ed. Butterworth-Heinemann, Elsevier, Oxford, 2nd edn, 2013, pp. 389–429.
75 Access Intelligence, Chemical Engineering, **https://www.chemengonline.com/pci-home**, (accessed 22 February 2025).
76 R. Williams Jr., *Chem. Eng.*, 1947, **54**, 124–125.
77 E. Rezaei and S. Dzuryk, *Chem. Eng. Res. Des.*, 2019, **144**, 354–369.
78 C. N. Hamelinck, A. P. C. Faaij, H. den Uil and H. Boerrigter, *Energy*, 2004, **29**, 1743–1771.
79 R. W. Whitesides, Process Equipment Cost Estimating by Ratio and Proportion, **https://www.pdhonline.com/courses/g127/g127content.pdf**, (accessed 22 February 2025).
80 W. L. Luyben, *Comput. Chem. Eng.*, 2017, **103**, 144–150.
81 P. Spath, A. Aden, T. Eggeman, M. Ringer, B. Wallace and J. Jechura, Biomass to Hydrogen Production Detailed Design and Economics Utilizing the Battelle Columbus Laboratory Indirectly-Heated Gasifier, Golden, CO, 2005.
82 S. Chiuta, N. Engelbrecht, G. Human and D. G. Bessarabov, *J. CO_2 Util.*, 2016, **16**, 399–411.
83 M. Luberti and H. Ahn, *Sep. Purif. Technol.*, 2021, **261**, 118254.
84 A. Paturska, M. Repele and G. Bazbauers, *Energy Procedia*, 2015, **72**, 71–78.
85 ISO, ISO 14044. International Standards Organization. Environmental Management - Life Cycle Assessment. Requirements and Guidelines; 2006, AENOR, Madrid, 2006.
86 ISO, ISO 14040:2006. Environmental management—Life cycle assessment—Principles and framework, ISO, Geneva, Second edition, 2006.
87 G. Cao, R. M. Handler, W. L. Luyben, Y. Xiao, C.-H. Chen and J. Baltrusaitis, *Energy Convers. Manage.*, 2022, **265**, 115763.
88 Eurostat, Shedding light on energy in Europe – 2024 edition, 2024.
89 European Commission, European Platform on LCA|EPLCA, **https://eplca.jrc.ec.europa.eu/LCDN/developerEF.html**, (accessed 19 October 2024).
90 Ellen MacArthur Foundation, Towards the Circular Economy, 2012.
91 M. Escribà-Gelonch, G. D. Butler, A. Goswami, N. N. Tran and V. Hessel, *Plant Physiol. Biochem.*, 2023, **196**, 917–924.
92 D-CRBN, **https://d-crbn.com/our-technology/**, (accessed 22 March 2024).
93 A. Yamamoto, S. Mori and M. Suzuki, *Thin Solid Films*, 2007, **515**, 4296–4300.
94 A. Anastasopoulou, R. Keijzer, S. Butala, J. Lang, G. Van Rooij and V. Hessel, *J. Phys. D: Appl. Phys.*, 2020, **53**, 234001.
95 M. S. Peters, K. D. Timmerhaus and R. E. West, *Plant Design and Economics for Chemical Engineers*, New York, 5th edn, 2003.
96 M. Fasihi and C. Breyer, *Energy Environ. Sci.*, 2024, **17**, 3503–3522.
97 P. Yue, Q. Fu, J. Li, X. Zhu and Q. Liao, *Green Chem.*, 2022, **24**, 2927–2936.
98 Z. Huang, R. G. Grim, J. A. Schaidle and L. Tao, *Energy Environ. Sci.*, 2021, **14**, 3664–3678.
99 O. S. Bushuyev, P. De Luna, C. T. Dinh, L. Tao, G. Saur, J. van de Lagemaat, S. O. Kelley and E. H. Sargent, *Joule*, 2018, **2**, 825–832.
100 M. Jouny, G. S. Hutchings and F. Jiao, *Nat. Catal.*, 2019, **2**, 1062–1070.
101 M. G. Kibria, J. P. Edwards, C. M. Gabardo, C.-T. Dinh, A. Seifitokaldani, D. Sinton and E. H. Sargent, *Adv. Mater.*, 2019, **31**, 1807166.
102 J. Lee, W. Lee, K. Ryu, J. Park, H. Lee, J. Lee and K. Park, *Green Chem.*, 2021, **23**, 2397–2410.
103 W. Li, J. T. Feaster, S. A. Akhade, J. T. Davis, A. A. Wong, V. A. Beck, J. B. Varley, S. A. Hawks, M. Stadermann, C. Hahn, R. D. Aines, E. B. Duoss and S. E. Baker, *ACS Sustainable Chem. Eng.*, 2021, **9**, 14678–14689.
104 M. J. Orella, S. M. Brown, M. E. Leonard, Y. Román-Leshkov and F. R. Brushett, *Energy Technol.*, 2020, **8**, 1900994.
105 M. Ramdin, B. De Mot, A. R. T. Morrison, T. Breugelmans, L. J. P. van den Broeke, J. P. M. Trusler, R. Kortlever, W. de Jong, O. A. Moultos, P. Xiao, P. A. Webley and T. J. H. Vlugt, *Ind. Eng. Chem. Res.*, 2021, **60**, 17862–17880.
106 W. Kuckshinrichs, T. Ketelaer and J. C. Koj, *Front. Energy Res.*, 2017, **5**, 1–13.
107 R. Šulc and P. Ditl, *J. Cleaner Prod.*, 2021, **309**, 127427.
108 G. D. Ulrich and P. T. Vasudevan, How to estimate utility costs, **https://terpconnect.umd.edu/~nsw/chbe446/HowToEstimateUtilityCosts-UlrichVasudevan2006.pdf**, (accessed 22 February 2025).
109 T. Nguyen, Z. Abdin, T. Holm and W. Mérida, *Energy Convers. Manage*, 2019, **200**, 112108.
110 F. Rosner, Q. Chen, A. Rao and S. Samuelsen, *Appl. Energy*, 2020, **277**, 115500.
111 A. Giuliano, C. Freda and E. Catizzone, *Bioengineering*, 2020, **7**, 1–18.
112 C. M. Plugge, *Microb Biotechnol.*, 2017, **10**, 1128–1130.

113 D. Heide, L. Von Bremen, M. Greiner, C. Hoffmann, M. Speckmann and S. Bofinger, *Renew Energy*, 2010, **35**, 2483–2489.
114 N. S. Matin and W. P. Flanagan, *Int. J. Hydrogen Energy*, 2024, **49**, 1405–1413.
115 C. L. Thiel, M. Eckelman, R. Guido, M. Huddleston, A. E. Landis, J. Sherman, S. O. Shrake, N. Copley-Woods and M. M. Bilec, *Environ. Sci. Technol.*, 2015, **49**, 1779–1786.
116 M. Bachmann, S. Völker, J. Kleinekorte and A. Bardow, *ACS Sustainable Chem. Eng.*, 2023, **11**, 5356–5366.
117 D. Frantzi and A. Zabaniotou, *Energies*, 2021, **14**, 7366.
118 J. Nisamaneenate, I. A. Idris, S. Tocharoen, D. Atong and V. Sricharoenchaikul, *Process Saf. Environ. Prot.*, 2024, **189**, 674–684.
119 N. Hajjaji, S. Martinez, E. Trably, J.-P. Steyer and A. Helias, *Int. J. Hydrogen Energy*, 2016, **41**, 6064–6075.

